Geochimica et Cosmochimica Acta 372 (2024) 154–170

Contents lists available at ScienceDirect

Geochimica et Cosmochimica Acta

journal homepage: www.elsevier.com/locate/gca

Fractionation of iron and titanium isotopes by ilmenite and the isotopic compositions of lunar magma ocean cumulates

Kelsey B. Prissel [a,*], Michael J. Krawczynski [a], Nicole X. Nie [b], Nicolas Dauphas [b], Sarah M. Aarons [b], Andy W. Heard [b], Michael Y. Hu [c], E. Ercan Alp [c], Jiyong Zhao [c]

[a] Department of Earth and Planetary Sciences, Washington University in St. Louis, 1 Brookings Drive, St. Louis, 63123, MO, USA
[b] Origins Laboratory, Department of Geophysical Sciences and Enrico Fermi Institute, The University of Chicago, 5734 South Ellis Avenue, Chicago, 60637, IL, USA
[c] Advanced Photon Source, Argonne National Laboratory, 9700 South Cass Avenue, Argonne, 60439, IL, USA

ARTICLE INFO

Associate editor: Shichun Huang

Keywords:
Ilmenite
Iron isotopes
Titanium isotopes
Lunar magma ocean
Mare basalts

ABSTRACT

Basaltic volcanism on the Moon produced low- and high-Ti mare basalt suites that are also distinct with respect to their iron, titanium, and magnesium isotopic compositions. Here, the equilibrium fractionation of Fe and Ti isotopes between ilmenite and melt was experimentally investigated in order to evaluate the role of ilmenite in generating the isotopic compositional variability among the lunar mare basalts. Ilmenite crystallization experiments were conducted using two bulk compositions: an ilmenite-saturated basaltic andesite and an ilmenite-saturated Apollo 14 black glass, and the Fe and Ti isotopic compositions of the experimental ilmenites and glass (quenched melt) were analyzed using solution MC-ICPMS after hand-picking. Additionally, Nuclear Resonant Inelastic X-ray Scattering (NRIXS) measurements on synthetic ilmenite were conducted and compared to previous NRIXS measurements on synthetic lunar glasses in order to derive temperature-dependent equilibrium ilmenite-melt Fe isotopic fractionations. Experimentally determined ilmenite-melt fractionations were then incorporated into a lunar magma ocean crystallization model that tracks the major element and isotopic compositional evolution of lunar magma ocean cumulates and residual liquid. There is good agreement between the Fe equilibrium isotopic fractionation measured by NRIXS and the laboratory equilibration experiments, and we find that the isotopic fractionation is sensitive to ilmenite compositional differences (0 vs. 10% Fe^{3+}). Further, the light Ti isotopic composition of ilmenite relative to the melt ($\Delta^{49}Ti_{ilmenite\text{-}melt} = -0.09 \pm 0.03‰$ at 1100 °C) is consistent with the higher coordination of Ti in ilmenite relative to melts and results of previous studies. The modeled Ti isotopic compositions for lunar magma ocean cumulates display Ti isotopic variability sufficient to explain the low- and high-Ti mare basalt sources. However, the difference in Fe isotopic composition between the low- and high-Ti mare basalts cannot be attributed solely to ilmenite fractionation. Instead, Fe isotopic fractionation by additional products of lunar magma ocean crystallization, such as clinopyroxene, is required to generate the inferred Fe and Mg isotopic variability in the lunar mantle. Alternatively, the Fe and Mg isotopic compositions of the lunar mare basalts may indicate Fe-Mg interdiffusion has occurred in the Ti-rich component of the mare basalt source regions via reaction between ilmenite cumulates and the olivine- and pyroxene-rich lunar mantle.

1. Introduction

The compositional variability observed among lunar volcanic samples, particularly with respect to titanium, demonstrates that the lunar mantle is heterogeneous and likely has large scale isotopic heterogeneities. Lunar mare basalts and ultramafic volcanic glasses, which represent melts of the lunar interior, are characterized by low- and high-Ti suites (Shearer et al., 2006). High-titanium mare basalts and volcanic glasses have compositions with 10 – 15 wt.% TiO_2 and greater, whereas a majority of terrestrial basalts contain less than 2 wt.% TiO_2 (Fig. 1, Basaltic Volcanism Study Project, 1981). The distinctive titanium enrichment in lunar magmas indicates that the nature of the mantle and melt generation processes on the Moon differ from those encountered on Earth.

* Corresponding author at: Jacobs, NASA Johnson Space Center, 2101 NASA Parkway, MailCode XI3, Houston, TX 77058, United States.
E-mail address: kelsey.prissel@nasa.gov (K.B. Prissel).

https://doi.org/10.1016/j.gca.2024.01.006
Received 7 February 2023; Accepted 5 January 2024
Available online 12 January 2024

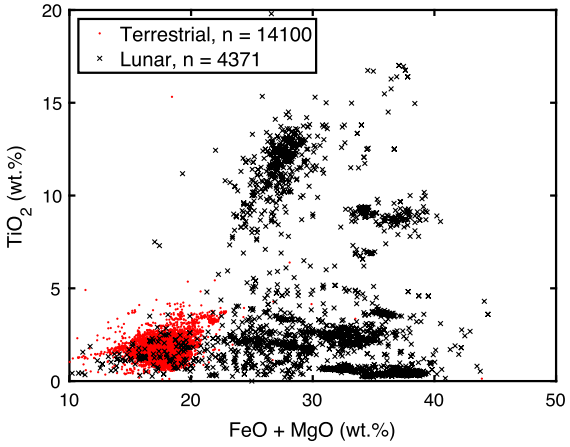

Fig. 1. Compositional variations between terrestrial mid-ocean ridge basalts (red dots) and lunar mare basalts and volcanic glasses (black crosses). Terrestrial data (14,100 samples) were downloaded from the PetDB Database (www.earthchem.org/petdb) using the following parameters: tectonic setting = spreading center and rock classification = basalt. Lunar data (4,371 samples) were downloaded from the database compiled by Clive Neal (www3.nd.edu/~cneal/Lunar-L/Mare-Basalt-Database.xls). The great diversity of mare basalt compositions reflects the heterogeneous nature of the lunar mantle inherited from lunar magma ocean crystallization.

The mantle source regions of the mare basalts are thought to be comprised of chemically diverse products of lunar magma ocean crystallization (e.g., Walker et al., 1975; Warren, 1985; Snyder et al., 1992). In general, there are three important compositional components in the mare basalt sources related to the products of a lunar magma ocean: ultramafic cumulates, high-titanium ilmenite-bearing cumulates, and a potassium-, rare earth element-, and phosphorus-rich component (KREEP) (e.g., Dickinson et al., 1985; Shervais et al., 1985; Neal et al., 1988; Snyder et al., 1992; Brown and Grove, 2015). Models of lunar magma ocean crystallization begin with estimates for a bulk Moon composition magma and precipitate olivine and orthopyroxene as the sole phases for more than 50% of crystallization (e.g., Snyder et al., 1992; Elkins-Tanton et al., 2011; Elardo et al., 2011). Though the relative mineral proportions are model dependent, these "ultramafic cumulates" are characterized by a mixture of olivine and orthopyroxene and likely make up the majority of the lunar mantle. In the late stages of lunar magma ocean crystallization after approximately 90% of the original magma has solidified, ilmenite, an Fe-Ti oxide, begins to crystallize, producing ilmenite-bearing cumulates. The KREEP component in the mare basalt sources is considered to be related to the residual liquid that remained toward the end of magma ocean solidification, as this component is highly enriched in incompatible elements that would not have partitioned strongly into the earlier crystallizing minerals olivine, orthopyroxene, clinopyroxene, ilmenite, and plagioclase. Of the three main compositional components in mare basalt sources, the ilmenite-bearing cumulates are most important in understanding the titanium variation between the source regions for the low- and high-Ti basalts.

Though ilmenite-bearing lunar magma ocean cumulates have often been invoked as the source of titanium enrichment in the lunar mantle, questions remain regarding the abundance and location of ilmenite in the lunar interior, as well as the processes responsible for incorporating ilmenite into the mantle sources of mare basalt magmas. Recent experimental studies of lunar magma ocean crystallization have provided improved constraints on when ilmenite precipitates and in what proportion relative to co-crystallizing minerals (Lin et al., 2017a,b; Charlier et al., 2018; Rapp and Draper, 2018; Lin et al., 2020). Minerals less dense than the coexisting liquid, such as plagioclase, are expected to float toward the lunar surface and aggregate to form a crust. In contrast, an ilmenite-rich cumulate layer is expected to sink through the lunar mantle due to its relatively high density (Hess and Parmentier, 1995). The feasibility and extent of ilmenite-bearing cumulate downwelling involves numerous geodynamic considerations (e.g., timing relative to magma ocean solidification, rheology of the lunar mantle, thickness of the ilmenite-bearing layer, proportion of ilmenite in the cumulate layer) (Dygert et al., 2016; Li et al., 2019; Zhao et al., 2019). In addition to lunar magma ocean processes, the mechanisms involved in the remelting of ilmenite-bearing cumulates and the ascent of dense high-Ti magmas must have influenced the nature, distribution, and volume of mare basalts of various kinds on the lunar surface (Wagner and Grove, 1997; Van Orman and Grove, 2000; Krawczynski and Grove, 2012; Vander Kaaden et al., 2015; Mallik et al., 2019).

High-precision, non-traditional stable isotope analyses of lunar samples can provide new constraints to test hypotheses regarding the nature of mare basalt sources. Resolvable differences in iron, titanium, and magnesium isotopic compositions exist between the low-Ti and high-Ti mare basalts. In the following, the Fe, Ti, and Mg isotopic compositions are expressed in δ-notations, which are permil departure of $^{56}Fe/^{54}Fe$, $^{49}Ti/^{47}Ti$, and $^{26}Mg/^{24}Mg$ ratios relative to reference materials IRMM-014, OL-Ti, and DSM3, respectively. For iron and titanium, the high-Ti mare basalts are isotopically "heavy" compared to low-Ti basalts (e.g., $\delta^{57}Fe_{high\text{-}Ti} = +0.274 \pm 0.020‰$, $\delta^{57}Fe_{low\text{-}Ti} = +0.127 \pm 0.012‰$; Poitrasson et al. (2019), and $\delta^{49}Ti_{high\text{-}Ti} = +0.009$ to $0.115‰$, $\delta^{49}Ti_{low\text{-}Ti} = -0.030$ to $0.055‰$; Millet et al. (2016); Kommescher et al. (2020)). In contrast for magnesium, high-Ti mare basalts are isotopically "light" relative to low-Ti basalts (e.g., $\delta^{26}Mg_{high\text{-}Ti} = -0.49 \pm 0.14‰$, $\delta^{26}Mg_{low\text{-}Ti} = -0.25 \pm 0.10‰$; Sedaghatpour et al. (2013)). Previous studies have concluded that the heavy Fe, heavy Ti, and light Mg isotopic compositions of the high-Ti mare basalts were inherited from ilmenite-bearing lunar magma ocean cumulates (Weyer et al., 2005; Liu et al., 2010; Craddock et al., 2010; Sedaghatpour et al., 2013; Wang et al., 2015; Sedaghatpour and Jacobsen, 2019). Recent studies have built upon these models, refining the petrologic interpretations of isotopic and trace element concentrations in lunar basalts, demonstrating the utility of non-traditional stable isotope systems in solving long-standing questions in lunar science (Kommescher et al., 2020; Rzehak et al., 2022). In general, ilmenite is hypothesized as a main control on the isotopic distinction observed between the low- and high-Ti mare basalts because it is the major Ti-bearing mineral in the lunar mantle.

In order to quantitatively evaluate the role of ilmenite in generating the isotopic variability among mare basalts, we experimentally investigated the equilibrium fractionation of Fe and Ti isotopes between ilmenite and melt. We developed a lunar magma ocean crystallization model that incorporates isotopic, minor element, and major element compositions in a coherent, fully mass-balanced way. Combining our ilmenite-melt isotopic fractionations with models of lunar magma ocean crystallization, we quantified the Fe, Ti, and Mg isotopic compositions of lunar magma ocean cumulates. We then determined whether ilmenite fractionation under equilibrium conditions can account for the observed isotopic compositions of the lunar mare basalts.

2. Materials and methods

2.1. Ilmenite crystallization experiments

Ilmenite crystallization experiments were conducted at Washington University in St. Louis using two bulk compositions: an ilmenite-saturated basaltic andesite, and an ilmenite-saturated Apollo 14 black glass (Table S1). The two starting compositions were chosen such that ilmenite would be the only Fe-bearing phase crystallized during the experiment. A basaltic andesite composition was investigated because lunar magmas will evolve to more Si-rich compositions as crystallization proceeds. Additionally, the solubility of TiO_2 in basaltic melts is extremely high, and thus, adding silica will influence the behavior of TiO_2 and provide a melt composition that is significantly different than the other composition (Apollo 14 black glass), and in this way allow us to look for a melt compositional effect on isotope fractionation.

Both starting materials were synthesized from a combination of oxide, carbonate, and titanate powders that were mixed under isopropanol in a silicon-nitride ball mill for 3 hours. Calcium was added as $CaCO_3$ for the basaltic andesite, and $CaTiO_3$ for the Apollo 14 black glass. Polyvinyl alcohol was added as a binding agent to the starting materials, and once dry, 75 mg aliquots were pressed into cylindrical pellets of 4 mm diameter and 2 mm height. Experiments on the basaltic andesite composition were conducted in one-atmosphere vertical gas-mixing furnaces with Re wire sample containers (Table 1), and experiments on the ilmenite-saturated Apollo 14 black glass were conducted in a piston cylinder apparatus using graphite sample capsules (Table 2). All phase abundances and Fe loss estimates were calculated using LIME (Prissel et al., 2023). Our experiments have been conducted at oxygen fugacities relevant to the oxygen conditions inferred for the Moon. These reducing conditions minimize the presence of Fe^{3+}, which has been demonstrated to affect Fe isotope fractionation (Section 3).

2.1.1. Ilmenite-saturated basaltic andesite

The ilmenite-saturated basaltic andesite starting composition was derived by adding additional TiO_2 to an evolved lunar basalt composition (Stadermann et al., 2022) in order to stabilize ilmenite as a liquidus phase. Ilmenite crystallization experiments on the basaltic andesite composition were conducted in one-atmosphere vertical gas-mixing furnaces at Washington University in St. Louis. The experiments were conducted for durations of 3-8 days (Table 1). A controlled flow of H_2 and CO_2 gases buffered the oxygen fugacity at approximately one log unit above iron-wüstite (f_{O_2} = IW+1) throughout each experiment. The fugacity was monitored with a Ca-doped zirconia oxygen probe using air as the reference gas. Starting material pellets were fused to rhenium loops and hung by a Pt wire thread in the furnace hot spot for the run duration. The reported run duration in Table 1 reflects the time between sample insertion and sample quench. Experimental samples were quenched rapidly by melting the Pt hanging wire and dropping the sample from within the furnace into a beaker of deionized water.

We conducted a series of preliminary experiments in order to determine a cooling sequence that would crystallize ilmenite grains suitable for hand-picking for isotopic analysis (Prissel, 2020). Each sample was inserted into the furnace at the starting temperature (T_{start}) and remained at that temperature for either 3 hours (experiments J045, H062, H063, J046) or 24 hours (experiments J047 and J109). The temperature of the furnace was then decreased to the final sample temperature (T_{final}) at a programmed cooling rate (see Table 1). Experiments H062 and J046 had an additional 24-hour dwell at 1123 °C in between T_{start} and T_{final}. The programmed cooling sequence promotes the nucleation of crystals, and slower cooling rates allow for more euhedral crystal growth (Hammer, 2006). We determined that a final temperature of approximately 1098 °C was necessary in order to crystallize a proportion of ilmenite sufficient for hand-picking and isotopic analysis. Additionally, the ilmenite grains from the experiments cooled at 1 °C/hr were thinner and more elongate than those in the experiments cooled at 0.5 °C/hr. Therefore, experiments J047 and J109, which cooled at a rate of 0.5 °C/hr and equilibrated at the final sample temperature for 2-3 days, were selected for isotopic analysis.

The experimental run products for the basaltic andesite composition contain glass, ilmenite, plagioclase, and a silica phase (Fig. 2). Ilmenite is present as euhedral grains with dimensions that range from 10 to 40 μm. The silica phase is present as subhedral, occasionally elongate grains that range from 10 to 60 μm in length. Plagioclase is present throughout the sample as patches of < 10 μm grains.

2.1.2. Ilmenite-saturated Apollo 14 black glass

The second starting composition, ilmenite-saturated Apollo 14 black glass, was created in order to conduct experiments in which ilmenite was the liquidus phase. Ilmenite and glass separation for isotopic analysis was aided by the sole crystalline phase being ilmenite.

We determined the starting composition for the ilmenite-only experiments by experimentally saturating an Apollo 14 black glass composition with synthetic ilmenite (Prissel, 2020). To do this, we began with a mixture of oxide and titanate powders that was prepared to be similar in composition to Apollo 14 black glass (Delano, 1986). We synthesized an ilmenite powder by mixing Fe sponge, Fe_2O_3, and TiO_2 in stochiometric proportions ($FeTiO_3$). Then, we loaded the synthetic black glass and ilmenite starting materials into a graphite capsule in a 2:1 mass ratio. The sample was heated to 1420 °C in a piston cylinder assembly at 10 kbar pressure for 24.1 hours. The experimental run products were analyzed for major element composition using the electron microprobe. The average composition of the quenched melt near the ilmenite-black glass interface was chosen as the target composition for our ilmenite-saturated Apollo 14 black glass starting material (Table S1).

Experiments on the ilmenite-saturated Apollo 14 black glass composition were conducted in a piston cylinder at Washington University in St. Louis. For each experiment, the starting material was packed into a graphite capsule with 4 – 4.5 mm height and approximately 0.75 mm wall thickness. The use of a graphite sample capsule promotes experimental oxygen fugacities at which minimal Fe^{3+} exists in the mineral and glass phases (approximately IW+1, Médard et al., 2008; Ni et al., 2021). Piston cylinder experiments were performed at 10 kbar pressure (Table 2). Experimental pressure was maintained during the experiment by an automatic pressure control system using the hot piston-in technique (Johannes et al., 1971). The sample temperature was 1350 °C and controlled to within 1 – 3 °C throughout the experiment, as monitored by a Eurotherm PID temperature controller. The offset between the thermocouple reading and sample temperature for the experimental assembly was calibrated using the spinel reaction-progress thermometer (Watson et al., 2002). The temperature gradient across the sample capsule is approximately 10 °C. Experiments were rapidly quenched by turning off the power to the apparatus. The reported experimental run durations (Table 2) reflect the time between reaching the experimental target temperature and quench. After the experiment, the sample capsule was cut in half and mounted in epoxy, then the cut face was polished in preparation for electron microprobe analysis.

The phase assemblage for the ilmenite-saturated Apollo 14 black glass experiments consists of ilmenite and glass (Fig. 2). Ilmenite is present as subhedral grains that range from 20 to 200 μm in diameter, with elongate ilmenite grains extending up to 500 μm in length. In addition to ilmenite and glass, patches of dendritic crystals are present toward the top of the experiment capsule (closest to the thermocouple). The dendritic texture of the crystals suggests they precipitated during quench. Additional experiments were conducted at 1400 °C and 1300 °C. The experiment at 1400 °C (F127) did not crystallize ilmenite, and the experiment at 1300 °C (F126) had a higher proportion of ilmenite crystals than those conducted at 1350 °C. The estimated phase abundances for ilmenite and glass in experiments F131 and F143 differ by approximately 10% (Table 2), and 3% of this difference can be attributed to the uncertainty of the phase abundance calculation. We observed a slight decrease (0.3%) in the average output power supplied to the apparatus during the last 4 hours of experiment F131; this change may explain the higher proportion of ilmenite in F131, as a decrease in output power would lower the sample temperature.

2.1.3. Assessment of equilibrium

The experimentally produced ilmenites are compositionally homogeneous as demonstrated by low standard deviations in the electron microprobe compositional analyses amongst the ilmenite grains in each sample (Table 3) and an absence of visible compositional zoning within the grains (Fig. 2). For both experimental approaches, we conducted replicate experiments in order to confirm that our experimental results and mineral separate techniques are repeatable and robust.

Our experimental run durations were designed to be long enough to fully equilibrate the ilmenite and glass in the measured samples. For instance, using the Fe-Mg interdiffusion data from Prissel et al. (2020),

Table 1
Run conditions and products for one-atmosphere gas-mixing furnace experiments conducted on the ilmenite-saturated basaltic andesite composition (Table S1). T_{start} is the temperature of the furnace when the sample was inserted. T_{final} is the temperature at which the experiment equilibrated after the furnace was decreased from T_{start} at the reported cooling rate.

Experiment	T_{start} (°C)	T_{final} (°C)	Cooling rate (°C/hr)	Time (hr)[a]	Phases (mode)	Δ IW[b]	% Fe loss[c]
J045	1177	1122	1.0	65	glass + silica	+0.8	
H062	1179	1098	1.0	144	glass (55) + silica (21) + plag (16) + ilm (8)	+0.7	7.8
H063	1149	1099	1.0	92	glass + silica + plag + ilm	+0.7	
J046	1178	1098	1.0	192	glass + silica + plag + ilm	+0.8	
J047	1122	1098	0.5	147	glass (55) + silica (23) + plag (15) + ilm (7)	+0.8	5.2
J109	1120	1097	0.5	116	glass (54) + silica (22) + plag (17) + ilm (7)	+0.9	4.4

The major element compositions of the phases in experiments J045, H063, and J046 were not analyzed, and thus there are no quantitative results for phase abundance or Fe loss to report.

[a] Reported time reflects the time elapsed between sample insertion and sample quench. For additional information on cooling rates and dwell times, see text Section 2.1.1.

[b] Oxygen fugacity is reported in log units relative to the iron-wüstite buffer.

[c] Percent Fe loss was estimated using the FeO content of the starting composition and the FeO content of the sample (calculated from the phase compositions and modal abundances using LIME; Prissel et al., 2023).

Table 2
Run conditions and products for piston cylinder experiments conducted on the ilmenite-saturated Apollo 14 black glass composition (Table S1).

Experiment	P (kbar)	T (°C)	Time (hr)	Phases (mode)	% Fe loss[a]
F127	10	1400	3.0	glass	
F126	10	1300	4.3	glass + ilm	
F128	10	1350	20.7	glass + ilm	
F131	10	1350	13.7	glass (74) + ilm (26)	−0.1
F143	10	1350	15.2	glass (82) + ilm (18)	0.0

The major element compositions of the phases in experiments F126, F127, and F128 were not analyzed, and thus there are no quantitative results for phase abundance or Fe loss to report.

[a] Percent Fe loss was estimated using the FeO content of the starting composition and the FeO content of the sample (calculated from the phase compositions and modal abundances using LIME; Prissel et al., 2023). No Fe loss/gain was detected within the uncertainty of the calculation.

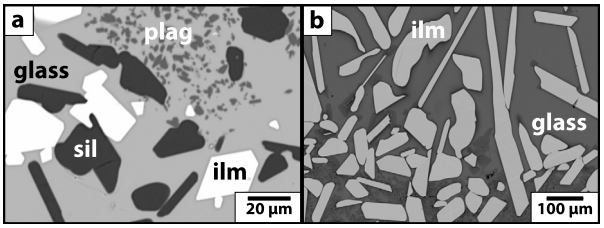

Fig. 2. Back-scattered electron image of two ilmenite crystallization experiments. a) Ilmenite-saturated basaltic andesite experiment J047 contains ilmenite (white, blocky crystals; “ilm”), a silica phase (dark gray, rounded crystals; “sil”), plagioclase (medium gray, small crystals; “plag”), and glass (bright gray matrix). b) Ilmenite-saturated Apollo 14 black glass experiment F131 contains ilmenite (bright gray crystals; “ilm”) and glass (gray matrix). Additionally, regions of quench crystals (dark gray) are observed toward the bottom of the capsule (bottom of image).

we calculated that at 1098 °C a 60 µm ilmenite grain will equilibrate with respect to Fe and Mg within an hour. Thus, in our experiments conducted at 1098 °C experiments with run durations of more than 100 hours, the major elements in the ilmenite samples would have had sufficient time to fully equilibrate. Assuming Ti diffusion in ilmenite is similar to that in titanomagnetite (Aggarwal and Dieckmann, 2002), the ilmenite grains would also be equilibrated with respect to Ti over our experiment durations. The Ti concentration in the silica phase is low (Table 3), and silica crystallization could potentially promote diffusive Ti isotopic fractionation (Chen et al., 2020). Using the Ti diffusivity in quartz (Cherniak et al., 2007) we calculated that 10 – 60 µm crystals crystallized at 1098 °C over run durations greater than 10 hours would not be sector zoned (Watson and Liang, 1995).

Loss of Fe during one-atmosphere gas-mixing furnace experiments has been shown to affect the Fe isotopic composition of experimental samples (Prissel et al., 2018). Though our experimental run durations were greater than four days, the one-atmosphere experiments (J047 and J109) only lost 5% of the initial Fe. Iron is lost to the Re wire during the experiment (Borisov and Jones, 1999; Prissel et al., 2018), and our isotopic measurements indicate that the wire is isotopically lighter than the melt (Table 4). Because we analyzed both the Fe concentration and the Fe isotopic composition of the Re wire, we can conclude that it did not have a significant effect on the isotopic mass balance of the sample as a whole (7.8 – 11 µg Fe). Additionally, at the high temperatures of our experiments, diffusion in the melt is rapid enough to equilibrate the sample as Fe partitions into the wire, and with time, the surface concentration of the wire eventually reaches an equilibrium value (see detailed analysis in Prissel et al., 2018). Given that metal sample containers (here, the Re wire) act as a reservoir for Fe in high-temperature experiments, we strongly recommend experimental isotopic fractionation studies analyze the Fe abundance and Fe isotopic composition of the metal container. The experimental samples synthesized using a graphite sample capsule in the piston cylinder did not experience measurable Fe loss (Table 2).

2.2. Electron microprobe analysis

Synthetic minerals and glasses from both sets of ilmenite crystallization experiments were analyzed for major element abundances using the JEOL JXA-8200 at Washington University in St. Louis. Standardization was performed with a beam diameter of 20 µm on natural and synthetic glass and mineral samples (synthetic Shankland forsterite, synthetic Mn-olivine, synthetic TiO_2, natural Ilmen Mountains ilmenite NMNH 96189, natural anorthite NMNH 137041, natural wollastonite, and natural Kakanui hornblende NMNH 143965). We used the mean

atomic number (MAN) method (Donovan et al., 2016) for wavelength dispersive spectrometer background correction and measured the following elements: Si, Al, Ti, Fe, Mn, Mg, Ca. Each quantitative analysis used a 15 kV accelerating potential and 25 nA beam current.

Glass compositions were analyzed with a 30 μm beam diameter for experiment F131, 10 μm beam diameter for experiments J047 and F143, and 5 μm beam diameter for experiment J109. Ilmenite compositions were analyzed with a 10 μm beam diameter for experiment F131, 2 μm beam diameter for experiment J109, and ~1 μm beam diameter for experiments J047 and F143. The silica phase was analyzed with a 2 μm beam diameter. Plagioclase was analyzed with ~1 μm beam diameter. Compositional data were reduced using Probe for EPMA software (https://www.probesoftware.com) and then filtered to exclude analyses where the analytical totals were less than 98.5 wt.% or greater than 101.5 wt.%. This threshold was expanded to include totals greater than 97 wt.% for J047 glass analyses, and totals less than 103 wt.% for silica phase and plagioclase analyses on experiment J109. Ilmenite analyses for experiments J047 and J109 were filtered to include only those where the cation total for 3 oxygen atoms was greater than 1.98 and less than 2.02 (ideal ilmenite stoichiometry contains 2 cations per 3 oxygen atoms). For experiments F131 and F143, ilmenite analyses contained 1.96-1.98 cations per 3 oxygen atoms. This cation deficiency is due to the relative excess of Ti in the ilmenite (Ti = 1.02 cations per 3 oxygen atoms). Averages of the analyzed glass and mineral compositions are reported in Table 3. The experimentally produced ilmenites are compositionally homogenous as demonstrated by low standard deviations in the electron microprobe compositional analyses amongst the ilmenite grains in each sample (Table 3) and an absence of visible compositional zoning within the grains (Fig. 2).

2.3. Sample dissolution and multicollector-inductively coupled plasma mass spectrometry (MC-ICPMS) methods

In order to determine the Fe isotopic fractionation factor between ilmenite and melt, we hand-separated ilmenite and glass (quenched melt) from the experimental run products and measured the Fe isotopic composition of each phase using solution MC-ICPMS. For each basaltic andesite experiment, the quenched experimental sample was crushed, select sample chips were mounted for electron microprobe analysis, and the rest of the material was allocated for isotopic analysis. For each Apollo 14 black glass experiment, half of the experiment capsule was mounted in epoxy for electron microprobe analysis, and after analysis it was extracted from the mount using a rotary tool. The recovered sample was then combined with the other half of the sample for isotopic analysis. Each of the experimental products was ground using a mortar and pestle, and the material was sieved to < 63 μm. Opaque ilmenite grains were hand-picked from the experimental samples under an optical microscope. The transparency of the glass allowed for separation of glass pieces that were free of crystals.

Ilmenite and glass separates were then dissolved in acid, purified for Fe through column chemistry, and analyzed for Fe and Ti isotopic composition using the Thermo Finnigan Neptune MC-ICPMS in the Origins Lab at the University of Chicago. The starting material powders, experiment wires, and "total samples" (experimental sample left after minor glass and ilmenite separate removal) were also dissolved and measured to aid in interpretation of the measured and bulk isotopic compositions. The Fe isotopic compositions are reported in Table 4 as δ^{56}Fe relative to the reference material IRMM-524, whose isotopic composition is identical to IRMM-014 (Craddock and Dauphas, 2011). Glass separates were first dissolved in a heated 2:1 mixture of concentrated HF-HNO_3 for 24 hours on a hot-plate set to 120 °C, then dried and re-dissolved in aqua regia (3:1 ratio of HCl-HNO_3). The aqua regia step was repeated to ensure a complete dissolution and to remove any HF used in the first step, as the presence of trace HF can cause problems in the Ti purification chromatography. The experiment wires were dissolved using 6M HCl on a hot plate set to 120 °C for 24 hours. Because ilmenite and Ti oxide can be resistant to acid dissolution, high-pressure Parr Bombs were used to dissolve ilmenite separates, "total samples", and starting material powders following a protocol similar to Craddock and Dauphas (2011). Each sample was loaded into a 6 ml Savillex PFA vial filled with 2.5 mL HF and 0.5 mL HNO_3. The sample vial was heated inside a 45 mL Parr Bomb at 170 °C for 3 days. After the bomb digestion step, each sample was dried out and then dissolved in aqua regia twice. All sample solutions were eventually dried and taken up in 6M HCl for Fe column chemistry. A fraction of each sample was taken for Fe column chemistry while the remaining sample solution was reserved for Ti column chemistry. Iron purification through column chemistry followed the routine method of the Origins Lab at the University of Chicago (e.g., Dauphas et al., 2004; Dauphas and Rouxel, 2006; Dauphas et al., 2009b). Briefly, sample solutions were loaded onto 1 mL anion resin AG1-X8 (200 − 400 mesh) columns in 6M HCl, matrix elements were eluted using 8 mL 6M HCl, and then Fe was recovered from the column using 9 mL 0.4M HCl. The iron isotopic compositions of the sample solutions were measured using the standard-bracketing method of Dauphas et al. (2009b), in wet plasma mode, using medium resolution to resolve ArO^+, ArN^+, and $ArOH^+$ interferences.

We also measured the Ti isotopic compositions of the experimental run products for one of the ilmenite crystallization experiments (J047). For Ti isotopic measurement, a titanium double spike (^{47}Ti–^{49}Ti) was added to each dissolved sample in a 48:52 spike-to-sample ratio based on the mass of titanium in the sample (Millet and Dauphas, 2014). The samples were then prepared for Ti isotopic measurement through ion-exchange chromatography following the Origins Lab protocols previously described in Millet et al. (2016); Greber et al. (2017); Johnson et al. (2019). Titanium isotopes were measured on a MC-ICPMS bracketed with standards that were doped with the same double spike mixture as the sample. The ^{48}Ti concentrations were matched within ±10% of the sample Ti concentration. Following a block of 5 samples, a clean blank solution was measured for on-peak baseline correction. The measurements were made on the peak shoulder to avoid interferences of ^{28}Si^{19}F on ^{47}Ti and ^{30}Si^{16}O on ^{46}Ti (Millet and Dauphas, 2014). Basalt geostandard BHVO-2 was processed simultaneously with the experimental samples, and the measured Ti isotopic composition (δ^{49}Ti= +0.019 ± 0.009‰) is in agreement with previously reported values (δ^{49}Ti= +0.020 ± 0.006‰, Millet et al. (2016), and δ^{49}Ti= +0.021 ± 0.020‰ Millet and Dauphas (2014)). The titanium isotopic compositions are reported as δ^{49}Ti relative to the Origins Laboratory Ti reference material (OL-Ti, Millet and Dauphas, 2014) (Table 5). Reported uncertainties (95% confidence interval) on the Ti isotopic compositions were determined using the methods described in Dauphas et al. (2009b) and incorporate both the measurement uncertainty and the long-term external reproducibility of the instrument.

2.4. Nuclear resonant inelastic X-ray scattering spectroscopy (NRIXS) of Fe equilibrium isotopic fractionation factors

In addition to the ilmenite crystallization experiments, the synchrotron radiation-based technique nuclear resonant inelastic X-ray scattering spectroscopy (NRIXS) was used to derive quantities needed for calculating equilibrium iron isotopic fractionation factors involving ilmenite. From the phonon excitation probability function, $S(E)$, or the partial phonon density of states, $g(E)$, itself derived from S, the iron reduced partition function ratios (β-factors) can be derived, which can be used to calculate Fe equilibrium isotopic fractionation between phases (e.g., Polyakov et al., 2005; Dauphas et al., 2012, 2014; Liu et al., 2017; Dauphas et al., 2018).

Assuming that the bonds are harmonic, the β-factor at high temperature (above 500 °C) is calculated as a function of the mean force constant of the iron bonds, $\langle F \rangle$ in N/m.

$$1000 \ln \beta = 2904 \frac{\langle F \rangle}{T^2} \quad (1)$$

Table 3
Electron microprobe analyses of experimental run products in oxide weight percent.

Experiment	Phase	n[a]	SiO_2	s.d.	TiO_2	s.d.	Al_2O_3	s.d.	FeO	s.d.	MnO	s.d.	MgO	s.d.	CaO	s.d.	Total
Ilmenite-saturated basaltic andesite																	
J047	glass	13	43.86	0.34	6.42	0.06	9.93	0.03	26.51	0.19	0.45	0.02	1.88	0.01	8.71	0.03	97.76
	ilmenite	18	b.d.		52.43	0.33	0.29	0.03	44.23	0.33	0.50	0.04	1.77	0.19	0.21	0.06	99.43
	silica	7	98.06	0.70	0.59	0.04	0.15	0.03	0.54	0.06	0.03	0.01	b.d.		0.09	0.01	99.46
	plagioclase	8	43.43	0.68	0.22	0.13	35.30	0.54	1.27	0.47	0.03	0.02	0.10	0.03	19.40	0.23	99.75
J109	glass	17	45.32	0.38	6.36	0.08	9.90	0.10	26.54	0.19	0.44	0.02	1.94	0.03	9.00	0.03	99.49
	ilmenite	15	0.23	0.10	52.21	0.68	0.31	0.04	44.62	0.21	0.52	0.02	1.80	0.06	0.26	0.12	99.95
	silica	8	100.83	0.66	0.60	0.04	0.21	0.12	0.53	0.10	b.d.		b.d.		0.11	0.04	102.3
	plagioclase	10	44.61	0.27	0.73	0.86	34.02	3.32	3.13	3.12	0.06	0.05	0.23	0.21	18.61	1.40	101.4
Ilmenite-saturated Apollo 14 black glass																	
F131	glass	61	32.62	0.69	17.58	0.87	7.21	0.16	31.22	0.44	0.37	0.02	5.68	0.18	4.67	0.11	99.34
	ilmenite	44	b.d.		56.37	0.15	0.78	0.02	38.45	0.18	0.29	0.02	4.96	0.03	0.03	0.01	100.9
F143	glass	26	29.28	0.65	21.14	0.71	6.53	0.15	31.68	0.41	0.36	0.02	5.74	0.25	4.34	0.11	99.05
	ilmenite	23	b.d.		57.38	0.23	0.85	0.02	37.03	0.23	0.28	0.02	5.11	0.04	0.05	0.02	100.7

b.d. indicates that the measured composition was below detection limit.

[a] Compositions are reported as an average of *n* analyses. Oxide measurements are reported with 1σ standard deviation in the adjacent "s.d." column.

Table 4
Iron isotopic compositions for each experiment. Reported values (‰) are the weighted averages and weighted uncertainties (95% confidence interval) of multiple measurements.

Sample	Starting Composition (Mix)	Starting Material				Glass				Ilmenite				Total Sample				Experiment Wire				
		δ^{56}Fe	2σ	δ^{57}Fe	2σ	δ^{56}Fe	2σ	δ^{57}Fe	2σ	δ^{56}Fe	2σ	δ^{57}Fe	2σ	δ^{56}Fe	2σ	δ^{57}Fe	2σ	µg Fe	δ^{56}Fe	2σ	δ^{57}Fe	2σ
J047	basaltic andesite (#38)	0.256	0.039	0.385	0.059	0.254	0.030	2.680	0.050	0.317	0.030	2.854	0.050	0.317	0.032	2.894	0.046	7.8	0.062	0.043	2.659	0.065
J109	basaltic andesite (#38)	*0.256*	*0.039*	*0.385*	*0.059*	0.399	0.030	0.761	0.054	0.404	0.029	0.687	0.053	0.321	0.042	0.612	0.067	11	0.305	0.042	1.011	0.067
F131	Apollo 14 black glass (#48)	0.267	0.027	0.376	0.039	0.280	0.023	0.425	0.033	0.238	0.022	0.342	0.032	0.304	0.031	0.468	0.043					
F143	Apollo 14 black glass (#48)	*0.267*	*0.027*	*0.376*	*0.039*	0.425	0.038	0.688	0.057	0.368	0.038	0.675	0.057	0.375	0.038	0.611	0.057					

For N measurements and i = 1,...N, the weighted averages and weighted uncertainties are calculated from the iron isotopic composition and standard deviation on each measurement (i) using the following equations: $w_i = 1/\sigma_i^2$, $\sigma_{\text{average}} = 1/\sqrt{\Sigma w_i}$, $\delta^{56}\text{Fe}_{\text{average}} = \Sigma(w_i \delta^{56}\text{Fe}_i)/\Sigma w_i$

Table 5
Titanium isotopic compositions for experiment J047. Reported uncertainties are 95% confidence interval.

Sample	δ^{49}Ti (‰)	n[a]
Starting Material	−0.144 ± 0.018	9
Glass	−0.140 ± 0.024	6
Ilmenite	−0.228 ± 0.021	9
Total Sample	−0.168 ± 0.013	9

[a] Number of repeated sample measurements.

Table 6
Mean force constants and coefficients of the $1/T^2$ polynomial expansion for iron beta-factors for synthetic ilmenite samples.

Sample	1000 x lnβ = A/T^2 + B/T^4 + C/T^6 (T in K)			
	<F> (N/m)	A (x10^5)	B (x10^9)	C (x10^{13})
ilm-2	156 ± 10	4.46 ± 0.28	−2.10 ± 0.47	3.29 ± 1.46
F144	193 ± 7	5.51 ± 0.21	−5.06 ± 0.62	20.43 ± 4.09
Apollo 16 Green[a]	189 ± 9	5.36 ± 0.26	−4.29 ± 0.68	12.34 ± 3.60
Apollo 17 Orange[a]	203 ± 11	5.79 ± 0.32	−4.90 ± 0.79	13.24 ± 3.81

[a] NRIXS data for synthetic Apollo 16 Green and Apollo 17 Orange glasses from Prissel et al. (2018).

At a given temperature, the equilibrium stable isotopic fractionation factor ($\alpha_{\text{mineral-melt}}$) between two phases is related to the β-factor and Fe isotopic composition (δ^{56}Fe) for each phase through:

$$1000 \ln \alpha_{\text{mineral-melt}} = \delta^{56}\text{Fe}_{\text{mineral, eq}} - \delta^{56}\text{Fe}_{\text{melt, eq}} = 1000 \ln \beta_{\text{mineral}} - 1000 \ln \beta_{\text{melt}} \quad (2)$$

The equilibrium iron isotopic fractionation between ilmenite and lunar melts can be calculated as a function of temperature using equations (1) and (2), the force constants for ilmenite determined in this work, and the force constants previously reported for a suite of synthetic lunar volcanic glasses (Prissel et al., 2018).

We synthesized ilmenite for NRIXS measurement at sector 3ID of the Advanced Photon Source. To perform the NRIXS measurements, which are only sensitive to the Mössbauer isotope ^{57}Fe, ^{57}Fe-enriched Fe_2O_3 powder (96.64% ^{57}Fe, Cambridge Isotopes) was used. The starting material for the ilmenite synthesis was created using a stoichiometric mixture (1:2) of $^{57}Fe_2O_3$ and TiO_2 powders. The oxide powders were mixed by hand with isopropanol in an agate mortar and pestle for 2 hours. Two ^{57}Fe-doped ilmenite syntheses were conducted. One synthesis (ilm-2) was conducted at Case Western Reserve University in a one atmosphere box furnace at 1201 °C for 122.1 hours. For this synthesis, the starting material was placed in a small SiO_2 glass tube which was vacuum sealed in a larger vacuum sealed SiO_2 glass tube. The second ^{57}Fe-doped ilmenite synthesis (F144) was conducted at Washington University in St. Louis in a piston cylinder at 15 kbar and 1140 °C for 65.7 hours. The sample starting material was loaded into a 7.9 mm tall graphite capsule with 0.75 mm wall thickness. Electron microprobe analysis of the experimental run products yielded an ilmenite composition of $Fe_{0.98}Ti_{1.01}O_3$ for sample ilm-2, and $Fe_{1.06}Ti_{0.97}O_3$ for sample F144. The Fe excess (> 1 cation per 3 oxygens) in F144 indicates the presence of ferric iron. Using Mössbauer spectroscopy (methods presented in Nie et al., 2021), we determined that approximately 10% of the Fe is present as Fe^{3+}.

3. Results

The measured Fe isotopic compositions of the experimental glass and ilmenite separates define an ilmenite-melt iron isotopic fractionation for each experiment (Table 4, Table 7, Fig. 3). Our experimental results for the ilmenite-saturated Apollo 14 black glass indicate that ilmenite is isotopically lighter than the co-existing glass ($\delta^{56}\text{Fe}_{\text{ilmenite}} - \delta^{56}\text{Fe}_{\text{glass}} = -0.04 \pm 0.03$‰ for F131 and -0.06 ± 0.05‰ for F143,

Table 7
Comparison of the ilmenite-melt Fe isotopic fractionations experimentally determined in this work. For each method, the reported uncertainty on the ilmenite-melt fractionation was calculated from the reported measurement uncertainties on ilmenite and glass.

Method	T (°C)	$\Delta^{56}\text{Fe}_{\text{ilmenite-melt}}$ (‰)
Ilmenite crystallization (F131)	1350	−0.04 ± 0.03
Ilmenite crystallization (F143)	1350	−0.06 ± 0.05
NRIXS (ilm-2): 156 ± 10 N/m[a]	1350	−0.04 ± 0.01
	1100	−0.05 ± 0.02
Ilmenite crystallization (J047)	1098	+0.06 ± 0.04
Ilmenite crystallization (J109)	1097	+0.01 ± 0.04
NRIXS (F144): 193 ± 7 N/m	1350	0.00 ± 0.01
	1100	+0.01 ± 0.02

[a] NRIXS fractionations have been calculated at the given temperatures using the force constants for ilmenite reported in this work and the force constant for synthetic Apollo 16 green glass reported in Prissel et al. (2018).

Table 7). In contrast, the results from our ilmenite-saturated basaltic andesite experiments indicate that the ilmenite would either not fractionate iron isotopes ($\delta^{56}\text{Fe}_{\text{ilmenite}} - \delta^{56}\text{Fe}_{\text{glass}} = +0.01 \pm 0.04$‰ for J109), or in the case of experiment J047, the ilmenite would be isotopically heavier than the glass ($\delta^{56}\text{Fe}_{\text{ilmenite}} - \delta^{56}\text{Fe}_{\text{glass}} = +0.06 \pm 0.04$‰).

In Table 6, we give the coefficients of the $1/T^2$ polynomial expansion of iron beta-factors from the NRIXS measurements on our synthetic ilmenite samples. At high temperature, the dominant control on Fe isotopic fractionation is the force constant (Dauphas et al., 2012), so we focus on this quantity hereafter. The force constants calculated from the NRIXS spectra on our synthetic ilmenites are 156 ± 10 N/m for ilm-2 and 193 ± 7 N/m for F144 (Table 6). We calculated ilmenite-melt Fe isotopic fractionations using the force constants for ilmenite reported in this work and the force constant for a synthetic Apollo 16 green glass reported in Prissel et al. (2018) (Table 7). The fractionation calculated from the NRIXS sample with less Fe^{3+} (ilm-2) agrees with the ilmenite-melt iron isotopic fractionations derived from the Apollo 14 black glass ilmenite crystallization experiments (Fig. 3). Our results for ilmenite with 10% Fe^{3+} (F144) are consistent with our basaltic andesite ilmenite crystallization experiments, as well as previously reported ilmenite-melt Fe isotopic fractionations deduced from experimental studies on ilmenite with 9.3% Fe^{3+} ($\delta^{56}\text{Fe}_{\text{ilmenite}} - \delta^{56}\text{Fe}_{\text{melt}} = -0.013$‰, Sossi and O'Neill, 2017).

Using the Ti isotopic compositions of our synthetic glass and ilmenite (Table 5), we determined an equilibrium ilmenite-melt Ti isotopic fractionation of $\Delta^{49}\text{Ti}_{\text{ilmenite-melt}} = -0.09 \pm 0.03$ at 1098 °C. This result is in excellent agreement with previous experimental results for lunar ilmenite-melt Ti isotopic fractionation at our experimental oxygen fugacity (Fig. 4; Rzehak et al., 2022). Previously, Millet et al. (2016) defined a temperature-dependent oxide-melt isotopic fractionation $\Delta^{49}\text{Ti}_{\text{oxide-melt}} = -0.23 \times \frac{10^6}{T^2}$. Calculating the $\Delta^{49}\text{Ti}_{\text{oxide-melt}}$ fractionation for the experimental temperature of 1098 °C yields $\Delta^{49}\text{Ti}_{\text{oxide-melt}} = -0.12$‰, which is also within the estimated uncertainty of our experimentally determined fractionation. Further, our experimentally determined ilmenite-melt Ti isotopic fraction is within range of that predicted from the temperature and melt SiO_2 composition of our experiment (Deng et al., 2019; Johnson et al., 2019). Consistent with our results and those of previous experimental studies, natural sample studies and first-principles calculations have concluded that ilmenite is isotopically lighter than the melt and coexisting silicates (Millet et al., 2016; Greber et al., 2017; Deng et al., 2019; Johnson et al., 2019; Wang et al., 2020; Aarons et al., 2021; Hoare et al., 2022).

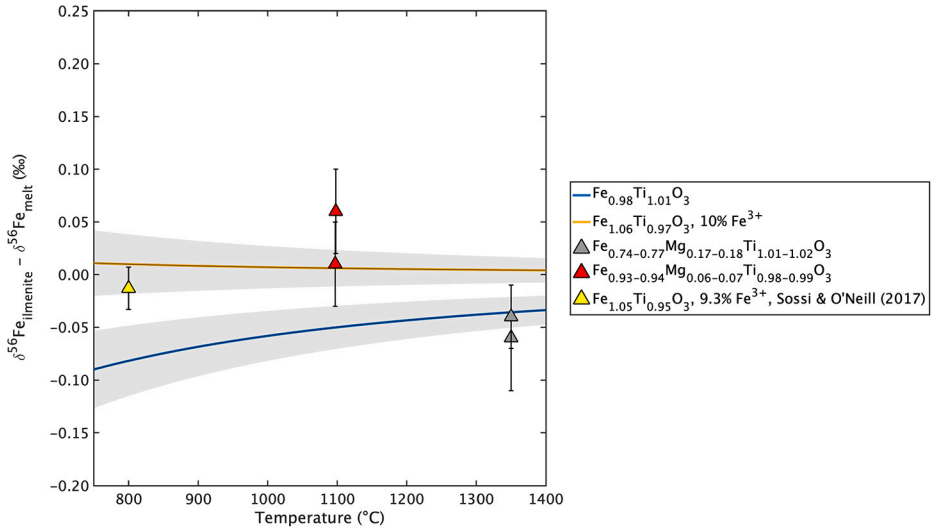

Fig. 3. Comparison of the ilmenite-melt Fe isotopic fractionations experimentally determined in this work and in Sossi and O'Neill (2017). The lines represent ilmenite-melt Fe isotopic fractionations calculated as a function of temperature using the NRIXS force constants for ilmenite reported in this work and the force constant for synthetic Apollo 16 green glass (189 ± 9 N/m) reported in Prissel et al. (2018). Ilmenite-melt fractionations determined from our ilmenite crystallization experiments are plotted as red and gray triangles at the experimental temperatures. The error bars represent a 95% confidence interval as calculated from the reported measurement uncertainties on ilmenite and glass. The differences between the two sets of crystallization experiments and the two NRIXS results reflect the Fe^{3+} compositional control on ilmenite-melt fractionation.

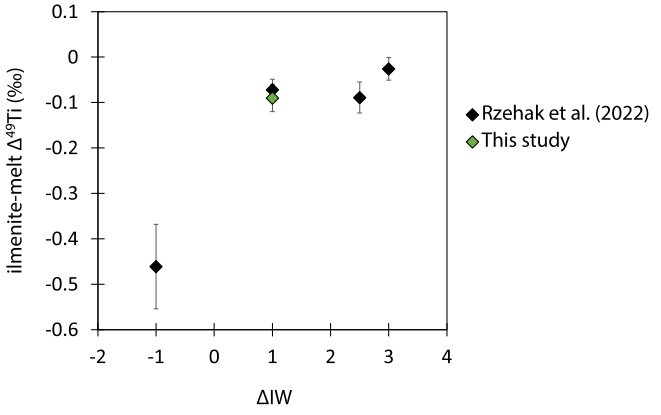

Fig. 4. Comparison of the ilmenite-melt Ti isotopic fractionations experimentally determined in this work (green) and in Rzehak et al. (2022) (black). Our result for ilmenite-melt Ti isotopic fractionation at f_{O_2} = IW+1 is consistent with that of Rzehak et al. (2022).

4. Discussion

4.1. Compositional controls on ilmenite-melt iron isotopic fractionation

The difference in calculated ilmenite-melt iron isotopic fractionation for the two sets of ilmenite crystallization experiments might be attributed to the silicate melt composition, the ilmenite composition, or the experimental oxygen fugacity. Melt composition and polymerization has been shown to affect iron isotope fractionation (Dauphas et al., 2014), and there is up to 16 wt.% difference in both SiO_2 and TiO_2 between the experiment glasses from the two sets of crystallization experiments (Table 3). However, we have previously determined that iron isotope fractionation would not be influenced by melt composition across this compositional range at f_{O_2} = IW (Prissel et al., 2018). The Apollo 14 black glass experiments crystallized ilmenite with more Ti and Mg (F131: $Fe_{0.77}Mg_{0.17}Ti_{1.01}O_3$, F143: $Fe_{0.74}Mg_{0.18}Ti_{1.02}O_3$) than those crystallized from the basaltic andesite (J047: $Fe_{0.94}Mg_{0.06}Ti_{0.99}O_3$, J109: $Fe_{0.93}Mg_{0.07}Ti_{0.98}O_3$). Further, the Ti excess (> 1 cation per 3 oxygens) in the Apollo black glass ilmenites may reflect a Ti^{3+} component, while the Ti deficit (< 1 cation per 3 oxygens) in the basaltic andesite ilmenites may indicate an Fe^{3+} component. All of these compositional factors (Mg, Fe^{3+}, Ti^{3+}) would affect the bonding of Fe in the ilmenite structure, and thus could affect the Fe isotopic fractionation (Teng et al., 2008; Dauphas et al., 2009a, 2014; Nie et al., 2021).

Ilmenite compositional control is further supported by our NRIXS results. Our NRIXS force constants for ilmenite provide an independent method for determining ilmenite-melt Fe isotopic fractionations. The NRIXS predicted ilmenite-melt equilibrium Fe isotopic fractionation is not the same depending on whether the value for ilm-2 or F144 is used because these two ilmenite measurements yield Fe force constants that do not overlap within error (Table 6, Table 7, Fig. 3). Importantly, these force constant values are not corrected for Fe^{3+} content, and as discussed in Section 2.4, ilmenite F144 has 10% Fe^{3+}. The force constant for hematite (244 N/M, Sturhahn et al., 1999) is significantly greater than those reported here for synthetic ilmenites, and it is likely that the force constant of ilmenite-hematite solid solution will increase with an increase in Fe^{3+} (Nie et al., 2021). An increased force constant with increased hematite component would explain the higher force constant for our synthetic ilmenite F144 with 10% ferric iron. Regardless of these differences, the predicted equilibrium isotopic fractionation between ilmenite and melt is small at magmatic temperatures and consistent with the results from our crystallization experiments (Fig. 3). Nevertheless, future studies on the effects of ilmenite composition and oxygen fugacity are required in order to conclusively determine why these experimental results differ.

The iron isotopic compositions of lunar mare basalt ilmenite separates suggest that ilmenite is isotopically heavier than coexisting silicates, though this relationship does not exist for every sample (Craddock et al., 2010). Our results may support relatively "heavy" ilmenite Fe isotopic compositions if crystallization occurred under conditions similar to that of our basaltic andesite experiments. Alternatively, if crystallizing silicates have "light" mineral-melt Fe isotopic fractionations, fractional crystallization of a mare basalt parental melt would lead to heavier melt Fe isotopic compositions prior to ilmenite saturation. In this case, ilmenite would be isotopically heavier than co-existing silicates regardless of which ilmenite-melt fractionation is used in the modeling. Importantly, our experimental ilmenite-melt fractionations enable quantitative models for compositional evolution at both the sample and magma ocean scale.

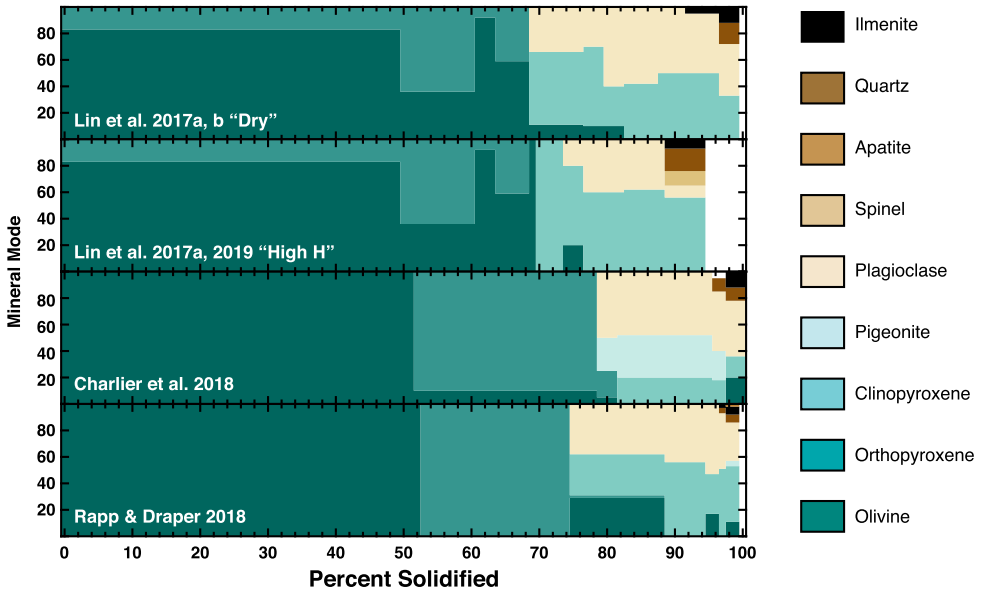

Fig. 5. Solidified lunar magma ocean phase assemblages determined by previous experimental studies (Lin et al., 2017a,b; Charlier et al., 2018; Rapp and Draper, 2018; Lin et al., 2020). For the Lin et al. models (top two bar charts): "Dry" summarizes the experimental results on a nominally anhydrous starting composition, while "High H" reflects an initial 3150 ppm H_2O in the starting lunar magma ocean composition. Charlier et al. (2018) results are those from experiments on the lunar primitive upper mantle (LPUM) composition (Table S2).

4.2. Isotopic composition of lunar magma ocean cumulates

In order to determine the isotopic composition of lunar magma ocean cumulates, we incorporated experimentally determined mineral-melt isotopic fractionations into models of lunar magma ocean (LMO) crystallization. Given our experimental focus on ilmenite in this study, we highlight the influence of ilmenite-melt isotopic fractionation on model results for the Fe and Ti isotopic compositions of LMO products. The onset of ilmenite crystallization is an important consideration for modeling the Fe and Ti isotopic composition of the lunar magma ocean. Experimental studies of lunar magma ocean crystallization have determined that ilmenite begins crystallizing near 88-98% LMO solidification (Lin et al., 2017a,b; Charlier et al., 2018; Rapp and Draper, 2018; Lin et al., 2020). These results are consistent with previous theoretical estimates for ilmenite saturation in the LMO (87-95% LMO solidification, Snyder et al., 1992; Elkins-Tanton et al., 2011), and the experimental mineral assemblages provide improved constraints on the major element evolution of the LMO that we incorporated in our model. As we are most interested in the compositional effects of ilmenite crystallization, only the experimental crystallization sequences that reach ilmenite saturation have been included here.

We developed a lunar magma ocean crystallization model that tracks both the major element chemistry and the isotopic composition of the minerals precipitating from the LMO and the residual LMO liquid. Our model begins with a given bulk composition for the lunar magma ocean (Table S2) and crystallizes according to the mineral phases and proportions determined by recent experimental studies (Fig. 5). Estimates for bulk silicate Moon isotopic composition define the initial isotopic compositions of the LMO liquid ($\delta^{56}Fe = +0.063 \pm 0.023‰$, Poitrasson et al. (2019); $\delta^{49}Ti = -0.003 \pm 0.014‰$, Millet et al. (2016), $\delta^{56}Mg = -0.26 \pm 0.16‰$, Sedaghatpour et al. (2013)). We have provided the mineral modes and compositions for each experimental LMO crystallization sequence, including those that do not reach ilmenite saturation (Elardo et al., 2011; Schmidt and Kraettli, 2022) in the Supplementary Material. Additional details about our crystallization model are also provided in Supplementary Material Section 1. This code is available on GitHub (https://github.com/kprissel/LMO) for future studies to model any of the 11 major elements and their isotopic evolution during LMO crystallization. Importantly, mineral-melt fractionations can be imposed for any of the 10 mineral phases reported in the experimental LMO models.

The mineral-melt isotopic fractionations used in our LMO models (Table S3) are a combination of those determined from our experimental results (Section 3) and data reported by previous studies (Dauphas et al., 2017; Sedaghatpour and Jacobsen, 2019; Rzehak et al., 2022). For Fe isotopes, we investigate two ilmenite-melt fractionations that encompass the variation in our experimental results ($\Delta^{56}Fe_{ilmenite\text{-}melt} = -0.06‰$ and $+0.06‰$). For the ilm-2 NRIXS sample, ilmenite-melt Fe isotopic fractionation calculated at 1000 °C also yields $\Delta^{56}Fe_{ilmenite\text{-}melt} = -0.06‰$. Though the LMO temperature will be higher at the onset of ilmenite crystallization, 1000 °C extends to the coldest temperatures of the previously published lunar magma ocean crystallization experiments (e.g., Charlier et al., 2018; Rapp and Draper, 2018). Mass-dependent isotopic fractionations are larger at lower temperatures, and thus the calculated fractionation represents a maximum fractionation between ilmenite and melt during ilmenite crystallization from the lunar magma ocean.

In addition to ilmenite-melt isotopic fractionation, we also present models that include mineral-melt isotopic fractionations for orthopyroxene, clinopyroxene, and pigeonite (Table S3). Previous investigations have concluded that olivine and pyroxene crystallization at lunar oxygen fugacities would not significantly fractionate iron isotopes ($\delta^{56}Fe_{melt} - \delta^{56}Fe_{mineral} < 0.02‰$, Sossi and O'Neill, 2017; Prissel et al., 2018). However, alternative models have imposed Fe and Mg mineral-melt isotopic fractionations for pyroxene crystallization during the lunar magma ocean (Sedaghatpour and Jacobsen, 2019; Wang et al., 2023; Jiang et al., 2023; Fu et al., 2023). Additionally for Ti, Rzehak et al. (2022) concluded that the best-fit models for Ti isotopic compositions of the mare basalts are those that also include mineral-melt isotopic fractionations for silicate minerals. In our LMO models, we incorporated orthopyroxene-melt and clinopyroxene-melt Fe isotopic fractionations from Sedaghatpour and Jacobsen (2019) and calculated a spinel-melt Fe isotopic fractionation at 1000 °C using the force constant for Fe^{2+} in MgFeAl spinel from Dauphas et al. (2017). For Ti, the ilmenite-melt and clinopyroxene-melt isotopic fractionations have been set equal to those reported by Rzehak et al. (2022) for oxygen fugacities of IW+1 and IW-1. We considered two cases for Mg: one in which Mg isotopes behave similar to Fe isotopes during crystallization

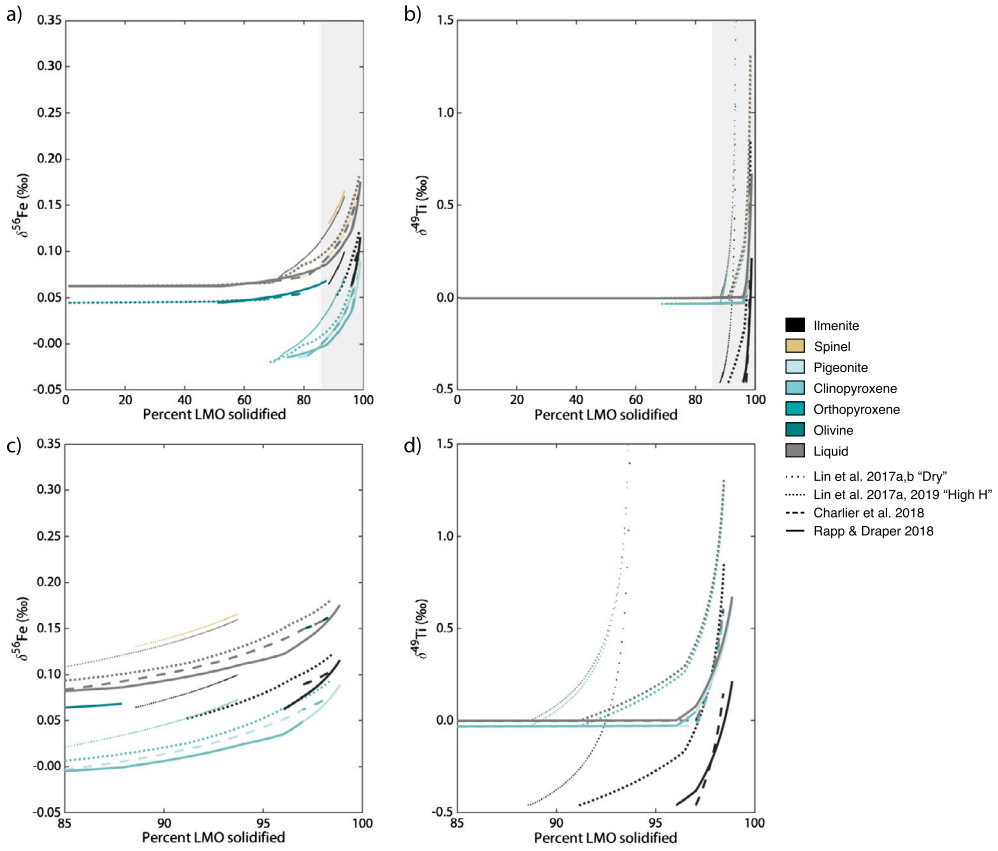

Fig. 6. Example model results for the iron (a,c) and titanium (b,d) isotopic compositional evolution of the lunar magma ocean liquid and mineral cumulates. The isotopic compositions of the LMO liquid and mineral products are plotted as a function of percent LMO solidified for each experimental crystallization sequence (see Fig. 5). Panes (b) and (d) highlight the isotopic evolution in the last 15% of lunar magma ocean crystallization when ilmenite begins to crystallize. In this model, ilmenite and the pyroxenes are isotopically lighter than the melt for both Fe and Ti isotopic fractionation, and spinel is heavier than the melt for Fe isotopic fractionation. No isotopic fractionation is imposed for the rest of the minerals, including olivine and plagioclase, and thus their isotopic composition would be equivalent to the liquid at the point of crystallization. The major element compositions for this model iteration are shown in Fig. 7d for Fe, and Fig. 8b for Ti.

(Schauble, 2011; Wang et al., 2020), and one that uses the mineral-melt isotopic fractionations from Sedaghatpour and Jacobsen (2019). The most important difference between these two approaches is that in the first approach, pyroxenes are isotopically lighter than the melt, and in the second approach, pyroxenes are isotopically heavier than the melt (Sedaghatpour and Jacobsen, 2019; Wang et al., 2023; Jiang et al., 2023; Fu et al., 2023). We assigned the clinopyroxene-melt isotopic fractionations to pigeonite in each LMO crystallization model.

An example LMO model result is given in Fig. 6. In this model, ilmenite, orthopyroxene, clinopyroxene, and pigeonite are isotopically lighter than the melt for Fe. Modeled ilmenite-melt and clinopyroxene-melt Ti isotopic fractionations are those for IW-1 from Rzehak et al. (2022). When fractionating minerals are isotopically lighter than the melt, lunar magma ocean crystallization drives the melt and subsequently crystallizing ilmenite and clinopyroxene toward heavier isotopic compositions. Toward the end of lunar magma ocean crystallization, fractionation of Fe and Ti isotopes by ilmenite and clinopyroxene leads to progressively heavier Fe and Ti isotopic compositions for both the ilmenite-bearing cumulates and the residual liquid. It is important to note that most of the ilmenite crystallized from the lunar magma ocean will have an isotopic composition toward the lower end of this modeled compositional range, as the heaviest ilmenites will only constitute a small fraction of the total ilmenite crystallized.

Models that impose mineral-melt isotopic fractionations for ilmenite, orthopyroxene, and clinopyroxene result in greater isotopic fractionation than those with only ilmenite-melt isotopic fractionations because at least one of the pyroxene phases is stable for a majority of lunar magma ocean crystallization (Fig. 5, Fig. 7). For example, with a "light" ilmenite-melt Fe isotopic fractionation and no pyroxene-melt Fe isotopic fractionation, our modeling results indicate that the ilmenites crystallizing from the lunar magma ocean would have Fe isotopic compositions δ^{56}Fe = 0.00 to 0.02‰ (Fig. 7b). When pyroxene-melt Fe isotopic fractionations are imposed, isotopic fractionation by pyroxene prior to ilmenite saturation can result in ilmenite with δ^{56}Fe = 0.05 to 0.12‰. In this model scenario, Fe isotopic fractionation by ilmenite and pyroxene results in a residual liquid with δ^{56}Fe = +0.18‰ (Fig. 6, Fig. 7d). For Ti, modeling mineral-melt isotopic fractionations for ilmenite and clinopyroxene at IW-1 leads to greater isotopic variability in the lunar magma ocean cumulates than at IW+1 (Fig. 8). For Mg isotopes, the choice of pyroxene-melt fractionation will dictate the Mg isotopic composition of modeled lunar magma ocean cumulates (Fig. 9).

4.3. Implications for mare basalt petrogenesis

Our LMO model provides new constraints for assessing whether LMO cumulate mixing can generate Fe, Ti, and Mg isotopic variability in the lunar mantle consistent with the inferred isotopic differences between the low-Ti and high-Ti mare basalt sources. Previous models for the isotopic composition of the ilmenite-bearing lunar magma ocean cumulates have invoked processes such as partial melting, fractional crystallization, or assimilation of ilmenite-bearing cumulates in order to explain the magnitude of Fe, Ti, and Mg isotopic fractionation in the lunar mantle (Millet et al., 2016; Sossi and O'Neill, 2017; Sedaghatpour and Jacobsen, 2019; Kommescher et al., 2020; Rzehak et al., 2022). Alternatively for Ti, the heavy Ti isotopic compositions of the high-Ti basalts have been explained by preferential sampling

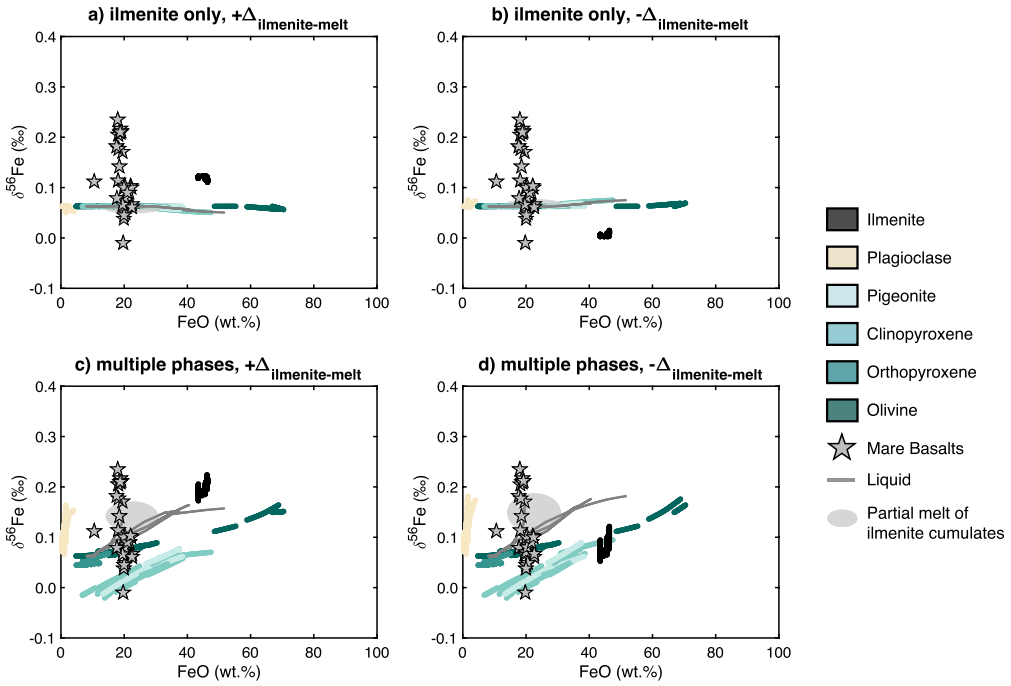

Fig. 7. Iron major element and isotopic composition for lunar magma ocean cumulates and liquids. In panes (a) and (b), ilmenite is the only mineral with an imposed iron isotopic fractionation. In panes (c) and (d), mineral-melt iron isotopic fractionations are imposed for ilmenite and the pyroxenes. Pyroxene mineral-melt iron isotopic fractionations are taken from Sedaghatpour and Jacobsen (2019). In panes (a) and (c), ilmenite is isotopically heavier than the melt ($\Delta^{56}Fe_{ilmenite\text{-}melt} = +0.06‰$), whereas in panes (b) and (d) ilmenite is isotopically lighter than the melt ($\Delta^{56}Fe_{ilmenite\text{-}melt} = -0.06‰$). Modeled phase compositions are colored according to the phase legend. Gray stars represent reported mare basalt compositions (Table S7). For each figure pane, the light gray ellipse encompasses calculated compositions for instantaneous melts of the ilmenites in that pane.

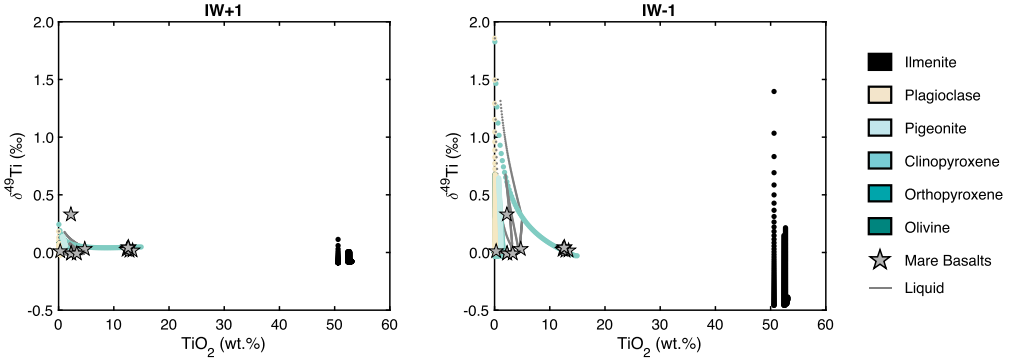

Fig. 8. Titanium major element and isotopic composition for lunar magma ocean cumulates and liquids. Mineral-melt fractionations for ilmenite and clinopyroxene are taken from Rzehak et al. (2022) for oxygen fugacities of IW+1 (a) and IW-1 (b). Modeled phase compositions are colored according to the phase legend. Gray stars represent reported mare basalt compositions (Table S7).

of late-crystallizing ilmenites that are heavier than the majority of ilmenite cumulates (Greber et al., 2017). Critically, isotopic variability within mare basalt sample suites is likely related to the crystallization and melting history of each sample (Kommescher et al., 2020; Rzehak et al., 2022), whereas here we focus on the first order compositional differences between the low-Ti and high-Ti mare basalt sources in the lunar mantle.

Our model results demonstrate that it is possible to generate ilmenite cumulates with Ti major element and isotopic compositions to explain the heavy Ti isotopic enrichment of the high-Ti mare basalts (Fig. 8). Given the magnitude of Ti isotopic fractionation during lunar magma ocean crystallization, it is possible to generate the Ti isotopic compositions of the high-Ti mare basalts by mixing ilmenite and silicate cumulates. Modeling LMO crystallization at lower oxygen fugacities leads to greater magnitudes of Ti isotopic fractionation toward the last 10% of crystallization (Fig. 8, Rzehak et al., 2022). For the reducing magmatic conditions on the Moon, there is a potential for Ti to exist as Ti^{3+}. Similar to our results for Fe, experimental studies on Ti isotopic fractionation in Fe-Ti oxides have demonstrated that oxygen fugacity, which determines Ti valence and coordination, has a strong influence on the Ti isotopic fractionation (Leitzke et al., 2018; Rzehak et al., 2021, 2022). An increased abundance of Ti^{3+} in either the melt or mineral phases could induce redox-driven fractionation of Ti isotopes. For instance, a melt preferentially concentrated in Ti^{4+} relative to Ti^{3+}-bearing minerals would be enriched in heavier Ti isotopes relative to the minerals (Leitzke et al., 2018). Modeled late-stage LMO liquid compositions are likely associated with the KREEP component in mare basalt sources. An isotopically heavy KREEP component is consistent with our results, previous models, and the Ti isotopic compositions of KREEP-rich lunar samples (Greber et al., 2017; Kommescher et al., 2020; Rzehak et al., 2022). Based on our modeling results for Ti, the isotopic composition of SaU 169 KREEPy impact melt breccia (δ^{49}Ti= +0.33‰, Greber et al. (2017)) supports an IW-1 LMO crystallization model (Fig. 8b). The

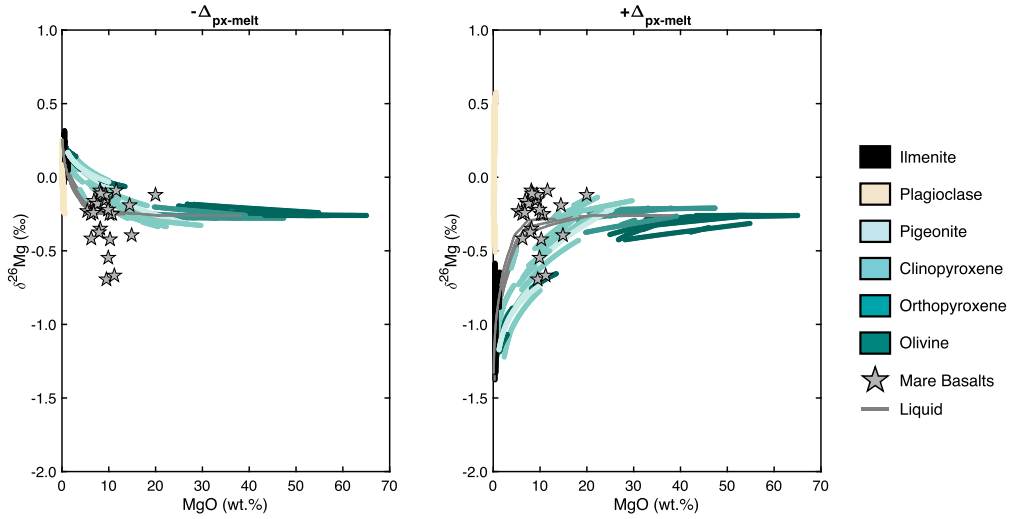

Fig. 9. Magnesium major element and isotopic composition for lunar magma ocean cumulates and liquids. In pane (a) pyroxene is isotopically lighter than the melt, with mineral-melt Mg isotopic fractionations set to be equal to those for Fe. In pane (b), pyroxenes are isotopically heavier than the melt with mineral-melt isotopic fractionations taken from Sedaghatpour and Jacobsen (2019). Modeled phase compositions are colored according to the phase legend. Gray stars represent reported mare basalt compositions (Table S7).

Ti isotopic compositions of LMO silicates and liquids do not reach the heavy values observed for Sau 169 when modeled at IW+1 (Fig. 8a).

Though our LMO model can generate Ti isotopic variability in the lunar mantle large enough to account for differences between the low- and high-Ti basalts, the magnitude of Fe isotopic enrichment in the high-Ti basalts cannot be explained solely by mixing lunar magma ocean cumulates (Fig. 7). Though the late-stage ilmenites and residual liquids get progressively heavier in Fe isotopic composition as the LMO crystallizes, the magnitude of this enrichment is not enough to match all of the high-Ti basalt iron isotopic compositions. This conclusion is robust for both ilmenite-melt Fe isotopic fractionations considered in our modeling. Models that incorporate pyroxene-melt isotopic fractionations generate greater isotopic variability in the lunar magma ocean cumulates, but still do not provide a compositional mixing space with which to produce the major element and isotopic compositions of the high-Ti mare basalts (Fig. 7c,d). Similarly for Mg isotopes, the mare basalt compositions cannot be explained by cumulate mixing when a light pyroxene-melt Mg isotopic fractionation is modeled (Fig. 9a). In contrast, models that employ a heavy pyroxene-melt Mg isotopic fractionation yield LMO cumulates that can be mixed to generate the Mg isotopic compositions of the mare basalts (Fig. 9b). Using pyroxene-melt Fe and Mg isotopic fractionations from Sedaghatpour and Jacobsen (2019) may be consistent with the Mg isotopic compositions of the mare basalts, but does not simultaneously explain the Fe isotopic compositions. Additionally, the model results and mare basalt compositional constraints in Fig. 9b require mixing with plagioclase cumulates to explain the Mg isotopic compositions, and the LMO plagioclase compositions rely on the modeled plagioclase-melt Mg isotopic fractionation (Sedaghatpour and Jacobsen, 2019).

Partial melting of ilmenite in the mare basalt source regions would fractionate isotopes between the melt and residue, provided that ilmenite was not exhausted from the source (Millet et al., 2016; Greber et al., 2017; Sossi and O'Neill, 2017; Kommescher et al., 2020; Rzehak et al., 2021). Using the equilibrium ilmenite-melt Fe isotopic fractionations determined in this work, we modeled partial melting of the model LMO ilmenites (Fig. 7). The first instantaneous melt will have the greatest Fe isotopic fractionation relative to the residue, and greater extents of melting will dilute this isotopic fractionation. Our experimentally determined ilmenite-melt isotopic fractionations also reveal that the magnitude of titanium isotopic fractionation during ilmenite melting would be greater than that for iron. We provide shaded fields on Fig. 7a-d that represent the compositions of the first partial melts of the modeled ilmenite cumulates for each ilmenite-melt Fe isotopic fractionation. Considering these partial melts and the LMO cumulates as potential mare basalt source components, the Fe isotopic compositions of the heaviest high-Ti basalts still cannot be reproduced by mixing. Thus, partial melting of LMO ilmenites alone is not a viable mechanism for generating the heavy Fe isotopic compositions of the high-Ti mare basalt parent magmas.

High-Ti mare basalt Fe isotopic compositions may be possible to explain by also invoking clinopyroxene-melt isotopic fractionation during clinopyroxene partial melting. Partial melting of both ilmenite and clinopyroxene is relevant because ilmenite-bearing LMO cumulates are also clinopyroxene-rich (e.g., Fig. 5, Van Orman and Grove, 2000). Our experimental results for ilmenite-melt Fe and Ti isotopic fractionation enable isotopic calculations for ilmenite melting, but additional data for clinopyroxene-melt Fe isotopic fractionation are needed to fully assess this possible mechanism. Additionally, our Fe isotopic fractionations for ilmenite were determined at IW+1. Given that ilmenite-melt and clinopyroxene-melt Ti isotopic fractionations are greater at IW-1 than at IW+1 (Fig. 4; Rzehak et al., 2022), the magnitude of mineral-melt Fe isotopic fractionation may vary across the range of lunar-relevant oxygen fugacities and ilmenite compositions (Section 4.1). Importantly, our results highlight the need to consider additional minerals and mechanisms when interpreting the Fe isotopic compositions of the high-Ti mare basalts.

4.4. Potential for diffusive isotopic fractionation in the lunar mantle

Two observations are critical in determining the origin of the iron isotopic compositions of mare basalts: 1) the Fe isotopic difference appears to be linked to the Ti major element compositional variability, and 2) high-Ti mare basalts, which have heavy Fe isotopic composition relative to low-Ti mare basalts, also have light Mg isotopic composition. At reducing conditions where Fe is predominantly Fe^{2+}, Fe and Mg isotopes should have a similar direction and magnitude of equilibrium fractionation (Schauble, 2011). Different directions and magnitudes for clinopyroxene-melt Fe and Mg isotopic fractionations could decouple the behavior of Fe and Mg isotopes in the lunar magma ocean (Sedaghatpour and Jacobsen, 2019; Jiang et al., 2023; Wang et al., 2023). Alternatively, here we consider diffusive exchange of Fe and Mg as a mechanism through which Fe and Mg isotopic fractionation would have opposite trends. In this case, the Fe and Mg isotopic compositions of the high-Ti component in mare basalt sources would indicate a non-

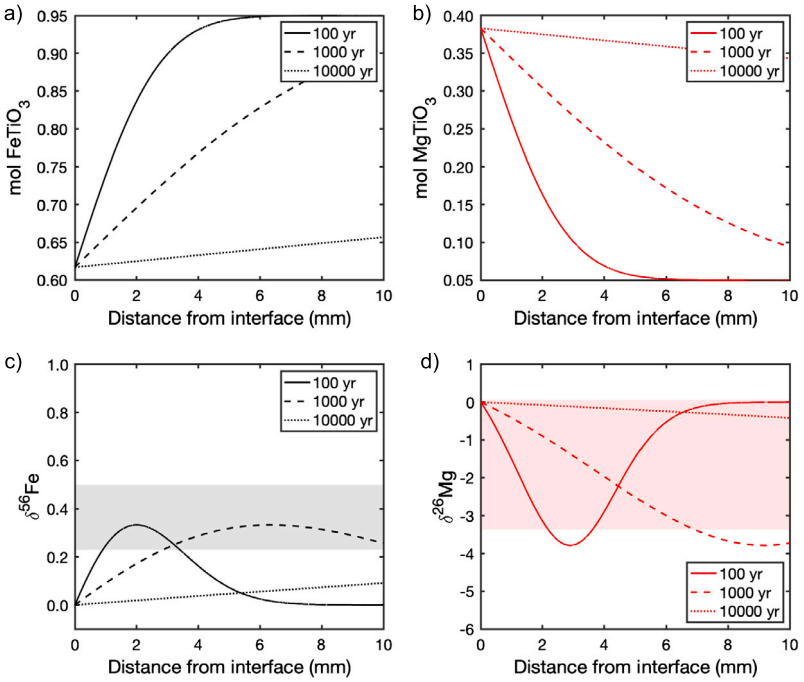

Fig. 10. Results from diffusive isotopic fractionation calculations for Fe-Mg interdiffusion in ilmenite at 800 °C after 100, 1000, and 10000 years. Diffusion of Fe out of ilmenite (a) creates an enrichment of heavy Fe isotopes in the ilmenite (c). Conversely, diffusion of Mg into ilmenite (b) leads to an enrichment of light Mg isotopes in the ilmenite (d). The shaded regions correspond to the range of isotopic compositions (‰) calculated for the ilmenite component in order to explain the isotopic compositions of the mare basalts, given in Table S7.

equilibrium isotopic fractionation took place. Because lighter isotopes of an element diffuse faster, diffusion of Mg into the high-Ti component of the mare basalt sources would produce lighter Mg isotopic compositions; conversely, diffusion of Fe out of this component would lead to heavier Fe isotopic compositions (e.g., Dauphas et al., 2010; Teng et al., 2011; Van Orman and Krawczynski, 2015). Additionally, the magnitude of diffusive isotopic fractionation would depend on the concentrations of Fe and Mg in the high-Ti component.

A potential method for inducing Fe-Mg interdiffusion in the high-Ti component of the mare basalt parent magmas is the chemical reaction between ilmenite-bearing lunar magma ocean cumulates and a lunar mantle comprised predominantly of olivine and pyroxene. Toward the end of lunar magma ocean crystallization, ilmenite-bearing cumulates are hypothesized to sink into the lunar mantle because these late-stage cumulates are more dense than the underlying cumulates consisting mainly of silicate minerals (e.g., Hess and Parmentier, 1995). Ilmenite in contact with an olivine and orthopyroxene cumulate can produce the Fe-Ti oxide mineral armalcolite via the subsolidus reaction

2FeTiO3 + MgSiO3 -> (Mg,Fe)2SiO4 + (Mg,Fe)Ti2O5

at depths less than 280 km in the lunar mantle (Thacker et al., 2009). As this chemical reaction progresses from left to right, Fe diffuses out of the oxide phase and into the silicate phase, and conversely, Mg diffuses out of the silicate phase and into the oxide phase. This Fe-Mg interdiffusion would produce heavier Fe isotopic compositions and lighter Mg isotopic compositions in the Fe-Ti oxide phase. At the onset of the reaction, the magnitude of Mg isotopic fractionation in the oxide would be greater than that of the Fe isotopic fractionation because the ilmenite begins with a composition that is nearly pure ilmenite ($FeTiO_3$). Additionally, titanium is not being diffusively exchanged in significant amounts in this reaction; therefore there would not be an associated Ti isotopic fractionation. Negative correlations have been previously observed for the measured Fe and Mg isotopic compositions of natural ilmenites sampled from terrestrial mafic intrusions (Chen et al., 2018; Tian et al., 2019). In these studies, the relationship between Fe and Mg isotopic compositions was attributed to diffusive isotopic fractionation involving subsolidus Fe-Mg exchange between ilmenite and silicate minerals. What we envision for ilmenite-rich mafic cumulates is different, as it would involve Fe-rich ilmenite reacting with Mg-rich pyroxene to make Fe-rich olivine and Mg-rich armalcolite. The reaction would form a mixed layer of olivine and armalcolite at the interface between ilmenite and pyroxene, and thus implicates the formation of both a new oxide phase and a new silicate phase. For the reaction to proceed, Fe needs to diffuse from ilmenite into pyroxene while Mg diffuses from pyroxene into ilmenite.

Modeling the reaction above is complicated by the fact that it involves phase transformation and moving boundaries. As a first pass on this question, we modeled Fe-Mg diffusive exchange between ilmenite and pyroxene using the diffusive fractionation equations given in Sio et al. (2018) and Fe-Mg interdiffusion coefficients for ilmenite from Prissel et al. (2020). To model diffusion-driven isotopic fractionation, the ratio of the diffusivities of coexisting isotopes is often given as $D_2/D_1 = (m_1/m_2)^b$, where b has a value between 0 and 0.5. The isotope effect for diffusion and b-parameter are not known for ilmenite, and thus we approximated $b_{Fe} = 0.2$ and $b_{Mg} = 0.1$ in order to have b values and $b_{Fe}/b_{Mg} = 2$, similar to that for olivine (Sio et al., 2018). The initial composition of the ilmenite (95 mol% $FeTiO_3$ and 5 mol% $MgTiO_3$) was chosen to be similar to the ilmenite compositions in lunar magma ocean crystallization experiments (Lin et al., 2017b; Charlier et al., 2018; Rapp and Draper, 2018; Lin et al., 2020). The interface composition of the ilmenite (61.7 mol% $FeTiO_3$ and 38.3 mol% $MgTiO_3$) was determined based on the partitioning of Fe and Mg between ilmenite and Fe-Mg silicates. We approximated $([Fe/Mg]_{pyroxene})/([Fe/Mg]_{ilmenite})$ to be 0.18 based on the values for olivine given in Thacker et al. (2009), and calculated the equilibrium ilmenite composition given a pyroxene with 10 mol% $FeSiO_3$. The Fe-Mg interdiffusion coefficient at 800 °C was calculated using the parameters given in Prissel et al. (2020). Beginning with an ilmenite isotopic composition δ^{56}Fe= 0‰ and δ^{26}Mg= 0‰, Fe-Mg interdiffusion can produce isotopic fractionation in ilmenite as large as δ^{56}Fe= +0.33‰ and δ^{26}Mg= −3.8‰ (Fig. 10). To a first approximation, we have demonstrated that the magnitude of Fe and Mg isotopic frac-

tionation required in the mare basalt sources can be produced by Fe-Mg interdiffusion in the Fe-Ti oxide cumulates.

Experimental investigations of the lunar mare basalts have concluded that the generation of high-Ti mare basalt parent magmas involves chemical reaction between a high-Ti component and mafic cumulates (e.g., Van Orman and Grove, 2000; Mallik et al., 2019). Mare basalt Ca isotope compositions also support reaction between low-Ti mantle sources and melts of ilmenite-bearing cumulates as a mechanism for generating high-Ti magmas (Klaver et al., 2021). The reaction proposed by Thacker et al. (2009) only occurs at depths less than 280 km in the lunar mantle, and these depths are consistent with those of the mare basalt sources (Shearer et al., 2006, and references therein). If shallow reaction between ilmenite cumulates and the lunar mantle is the process that generated the isotopic variability of the lunar mare basalts, then a similar isotopic signature and correlation with Ti may be absent from the lunar volcanic glasses, which are sourced from greater depth (Krawczynski and Grove, 2012). In support of this mechanism, the isotopic compositions of high-Ti (~ 9 wt.% TiO_2) Apollo 17 orange glass sample 74220 are similar to those of low-Ti mare basalts (δ^{56}Fe= 0.10 ± 0.06‰ Weyer et al. (2005), δ^{26}Mg= −0.19 ± 0.03‰ Sedaghatpour et al. (2013)). Here we have developed a model that explains the general Fe, Mg, and Ti isotopic differences observed between the low-Ti and high-Ti mare basalt suites. It is important to recognize that intra-suite isotopic variability will be influenced by additional factors and processes, such as changes in oxygen fugacity, fractional crystallization, and partial melting (Leitzke et al., 2018; Sedaghatpour and Jacobsen, 2019; Kommescher et al., 2020; Rzehak et al., 2021).

Though these diffusive processes occur at the grain scale, there is also potential for net diffusion at a regional scale during cumulate mantle overturn, and the magnitude of diffusive fractionation for Fe and Mg isotopes is important to consider in interpreting the isotopic compositions of igneous samples. If Fe-Mg interdiffusion between downwelling ilmenite-bearing lunar magma ocean cumulates and the olivine-, pyroxene-rich lunar mantle produced the heavy Fe isotopic composition of the high-Ti component in the mare basalt parental melts, then a complementary ultramafic component with a relatively light Fe isotopic composition may also exist in the lunar mantle. In addition to lunar magma ocean processes, the model we present here for Fe-Mg interdiffusion and isotopic fractionation between co-existing silicate and oxide phases can be applied to determining the cooling history of samples such as lunar dunite 72415. The measured iron isotopic compositions of lunar dunite 72415 are consistently the lightest Fe isotopic compositions measured for any lunar sample (δ^{56}Fe= −0.4 ± 0.1‰, Wang et al., 2015; Sossi and Moynier, 2017; Poitrasson et al., 2019). Given that equilibrium olivine crystallization does not fractionate Fe isotopes at lunar conditions (Prissel et al., 2018), the Fe isotopic signature of the lunar dunite likely represents diffusive isotopic fractionation. Additional insight into this diffusive re-equilibration will require petrographic and in-situ isotopic study of minerals within the dunite (e.g., Sio et al., 2013; Sio and Dauphas, 2017). Ultimately, natural sample observations and experimental isotopic fractionations highlight the need to consider diffusive fractionation when interpreting the stable isotopic compositions of lunar samples (Poitrasson et al., 2019).

5. Conclusions

1. We experimentally investigated the equilibrium fractionation of Fe and Ti isotopes between ilmenite and melt in order to evaluate the role of ilmenite in generating the isotopic compositional variability among lunar mare basalts. Our experimentally determined ilmenite-melt isotopic fractionations for Fe and Ti indicate that ilmenite would most likely be isotopically lighter than co-existing melt at lunar conditions (e.g., $\Delta^{56}Fe_{ilmenite\text{-}melt} = -0.05 \pm 0.02$‰ and $\Delta^{49}Ti_{ilmenite\text{-}melt} = -0.09 \pm 0.03$‰ at 1100 °C). For Fe, we found that the chemistry of ilmenite and the glass, as well as the redox state of iron, affect the strength of iron bonds and readily produce changes in this fractionation value.
2. We incorporated our Fe and Ti ilmenite-melt isotopic fractionations into fully mass balanced models of lunar magma ocean crystallization, and in doing so have estimated the Fe and Ti isotopic compositions of the LMO ilmenite cumulates and residual liquid. The modeled major element and isotopic compositions of lunar magma ocean cumulates provide new constraints for the compositions of mare basalt source regions. We determined that the Ti isotopic compositional differences between the low- and high-Ti mare basalt suites can be generated by mixing lunar magma ocean cumulates. However, the difference between the Fe isotopic compositions of the low- and high-Ti basalts cannot be explained by the Fe isotopic compositions of the modeled lunar magma ocean cumulates or ilmenite partial melting. Our model results suggest an additional mechanism or mineral, such as clinopyroxene, is involved in generating the heavy Fe isotopic compositions of the high-Ti mare basalts.
3. We propose that the heavy Fe and light Mg isotopic compositions of the high-Ti mare basalts reflects Fe-Mg interdiffusion in the Ti-rich component of the mare basalt sources. Diffusive exchange of Fe and Mg via subsolidus reaction between ilmenite cumulates and the olivine- and pyroxene-rich lunar mantle to make armalcolites at depths less than 280 km can explain the measured Fe, Ti, and Mg isotopic compositions of the low- and high-Ti mare basalts.

Our results highlight the importance of integrating multiple isotopic systems and major element constraints in models for lunar magma ocean crystallization and mare basalt petrogenesis. New experimental ilmenite-melt Fe and Ti isotopic fractionations enable future studies on the compositional variability of ilmenite-bearing igneous samples and diffusive isotopic fractionation in ilmenite. Specifically, these fractionations can be incorporated into quantitative crystallization and melting calculations for lunar magmas to investigate the isotopic variability within mare basalt sample suites (Kommescher et al., 2020; Rzehak et al., 2022; Jiang et al., 2023). Further, our lunar magma ocean model can be extended to investigate major element and isotopic compositional variability for 11 major elements and 10 mineral phases during lunar magma ocean crystallization.

CRediT authorship contribution statement

Kelsey B. Prissel: Conceptualization, Data curation, Formal analysis, Funding acquisition, Investigation, Methodology, Software, Visualization, Writing – original draft, Writing – review & editing. **Michael J. Krawczynski:** Conceptualization, Data curation, Funding acquisition, Methodology, Supervision, Writing – review & editing. **Nicole X. Nie:** Formal analysis, Investigation, Methodology, Writing – review & editing, Software. **Nicolas Dauphas:** Conceptualization, Data curation, Funding acquisition, Methodology, Supervision, Writing – review & editing, Software. **Sarah M. Aarons:** Investigation, Methodology, Writing – review & editing. **Andy W. Heard:** Investigation, Writing – review & editing. **Michael Y. Hu:** Formal analysis, Investigation, Methodology, Writing – review & editing, Data curation. **E. Ercan Alp:** Formal analysis, Investigation, Methodology, Writing – review & editing. **Jiyong Zhao:** Formal analysis, Investigation, Methodology, Writing – review & editing.

Declaration of competing interest

The authors declare that they have no known competing financial interests or personal relationships that could have appeared to influence the work reported in this paper.

Data availability

Data and model files are available through GitHub at https://github.com/kprissel/LMO.

Acknowledgements

This work was supported by NASA Earth and Space Sciences Fellowship Grant number 80NSSC17K0476 to KBP, NASA grants NNX17AE86G, NNX17AE87G, 80NSSC17K0744, 80NSSC20K0821, and NSF grant EAR-2001098 to ND, and the JETS-II contract at NASA Johnson Space Center. The authors would like to thank Paul Carpenter for his assistance with electron microprobe analysis. Additionally, the authors thank Hairuo Fu and three anonymous reviewers for insightful comments and suggestions that improved the manuscript, and Shichun Huang for thoughtful editorial handling. This research used resources of the Advanced Photon Source, a U.S. Department of Energy (DOE) Office of Science user facility at Argonne National Laboratory and is based on research supported by the U.S. DOE Office of Science-Basic Energy Sciences, under Contract No. DE-AC02-06CH11357.

Appendix A. Supplementary material

Additional details are provided for the lunar magma ocean crystallization model (Section 1) and the mare basalt source component mixing model (Section 2). Supplementary tables and figures are provided to complement the information presented in the main text. Further, an Excel spreadsheet ("LMO-PCS-modes.xlsx") is provided that contains mineral modes and compositions for the referenced LMO experimental studies.

Supplementary material related to this article can be found online at https://doi.org/10.1016/j.gca.2024.01.006.

References

Aarons, S.M., Dauphas, N., Blanchard, M., Zeng, H., Nie, N.X., Johnson, A.C., Greber, N.D., Hopp, T., 2021. Clues from ab initio calculations on titanium isotopic fractionation in tholeiitic and calc-alkaline magma series. ACS Earth Space Chem. 5, 2466–2480.

Aggarwal, S., Dieckmann, R., 2002. Point defects and cation tracer diffusion in $(Ti_xFe_{(1-x)})_{3-\delta}O_4$ 1. Non-stoichiometry and point defects. Phys. Chem. Miner. 29, 695–706.

Basaltic Volcanism Study Project, 1981. Basaltic Volcanism on the Terrestrial Planets. Pergamon Press, Inc.

Borisov, A., Jones, J.H., 1999. An evaluation of Re, as an alternative to Pt, for the 1 bar loop technique: an experimental study at 1400 °C. Am. Mineral. 84, 1528–1534.

Brown, S.M., Grove, T.L., 2015. Origin of the Apollo 14, 15, and 17 yellow ultramafic glasses by mixing of deep cumulate remelts. Geochim. Cosmochim. Acta 171, 201–215.

Charlier, B., Grove, T.L., Namur, O., Holtz, F., 2018. Crystallization of the lunar magma ocean and the primordial mantle-crust differentiation of the Moon. Geochim. Cosmochim. Acta 234, 50–69.

Chen, L.M., Teng, F.Z., Song, X.Y., Hu, R.Z., Yu, S.Y., Zhu, D., Kang, J., 2018. Magnesium isotopic evidence for chemical disequilibrium among cumulus minerals in layered mafic intrusion. Earth Planet. Sci. Lett. 487, 74–83.

Chen, X., Wang, W., Zhang, Z., Nie, N.X., Dauphas, N., 2020. Evidence from ab initio and transport modeling for diffusion-driven zirconium isotopic fractionation in igneous rocks. ACS Earth Space Chem. 4, 1572–1595.

Cherniak, D., Watson, E., Wark, D., 2007. Ti diffusion in quartz. Chem. Geol. 236, 65–74.

Craddock, P.R., Dauphas, N., 2011. Iron isotopic compositions of geologic reference materials and chondrites. Geostand. Geoanal. Res. 35, 101–123.

Craddock, P.R., Dauphas, N., Clayton, R., 2010. Mineralogical control on iron isotopic fractionation during lunar differentiation and magmatism. In: Lunar and Planetary Science Conference, p. 1230.

Dauphas, N., Craddock, P.R., Asimow, P.D., Bennett, V.C., Nutman, A.P., Ohnenstetter, D., 2009a. Iron isotopes may reveal the redox conditions of mantle melting from archean to present. Earth Planet. Sci. Lett. 288, 255–267.

Dauphas, N., Hu, M.Y., Baker, E.M., Hu, J., Tissot, F.L., Alp, E.E., Roskosz, M., Zhao, J., Bi, W., Liu, J., et al., 2018. SciPhon: a data analysis software for nuclear resonant inelastic X-ray scattering with applications to Fe, Kr, Sn, Eu and Dy. J. Synchrotron Radiat. 25, 1581–1599.

Dauphas, N., Janney, P.E., Mendybaev, R.A., Wadhwa, M., Richter, F.M., Davis, A.M., van Zuilen, M., Hines, R., Foley, C.N., 2004. Chromatographic separation and multicollection-ICPMS analysis of iron. Investigating mass-dependent and -independent isotope effects. Anal. Chem. 76, 5855–5863.

Dauphas, N., John, S.G., Rouxel, O., 2017. Iron isotope systematics. Rev. Mineral. Geochem. 82, 415–510.

Dauphas, N., Pourmand, A., Teng, F.Z., 2009b. Routine isotopic analysis of iron by HR-MC-ICPMS: how precise and how accurate? Chem. Geol. 267, 175–184.

Dauphas, N., Roskosz, M., Alp, E.E., Golden, D., Sio, C.K., Tissot, F.L., Hu, M.Y., Zhao, J., Gao, L., Morris, R., 2012. A general moment NRIXS approach to the determination of equilibrium Fe isotopic fractionation factors: application to goethite and jarosite. Geochim. Cosmochim. Acta 94, 254–275.

Dauphas, N., Roskosz, M., Alp, E.E., Neuville, D., Hu, M.Y., Sio, C.K., Tissot, F.L., Zhao, J., Tissandier, L., Médard, E., Cordier, C., 2014. Magma redox and structural controls on iron isotope variations in Earth's mantle and crust. Earth Planet. Sci. Lett. 398, 127–140.

Dauphas, N., Rouxel, O., 2006. Mass spectrometry and natural variations of iron isotopes. Mass Spectrom. Rev. 25, 515–550.

Dauphas, N., Teng, F.Z., Arndt, N.T., 2010. Magnesium and iron isotope in 2.7 Ga Alexo komatiites: mantle signatures, no evidence for Soret diffusion, and identification of diffusive transport in zoned olivine. Geochim. Cosmochim. Acta 74, 3274–3291.

Delano, J.W., 1986. Pristine lunar glasses: criteria, data, and implications. J. Geophys. Res. 91, D201–D213.

Deng, Z., Chaussidon, M., Savage, P., Robert, F., Pik, R., Moynier, F., 2019. Titanium isotopes as a tracer for the plume or island arc affinity of felsic rocks. Proc. Natl. Acad. Sci. 116, 1132–1135.

Dickinson, T., Taylor, G., Keil, K., Schmitt, R.A., Hughes, S., Smith, M., 1985. Apollo 14 aluminous mare basalts and their possible relationship to KREEP. J. Geophys. Res., Solid Earth 90, C365–C374.

Donovan, J.J., Singer, J.W., Armstrong, J.T., 2016. A new EPMA method for fast trace element analysis in simple matrices. Am. Mineral. 101, 1839–1853.

Dygert, N., Hirth, G., Liang, Y., 2016. A flow law for ilmenite in dislocation creep: implications for lunar cumulate mantle overturn. Geophys. Res. Lett. 43, 532–540.

Elardo, S.M., Draper, D.S., Shearer Jr, C.K., 2011. Lunar Magma Ocean crystallization revisited: bulk composition, early cumulate mineralogy, and the source regions of the highlands Mg-suite. Geochim. Cosmochim. Acta 75, 3024–3045.

Elkins-Tanton, L.T., Burgess, S., Yin, Q.Z., 2011. The lunar magma ocean: reconciling the solidification process with lunar petrology and geochronology. Earth Planet. Sci. Lett. 304, 326–336.

Fu, H., Jacobsen, S.B., Sedaghatpour, F., 2023. Moon's high-energy giant-impact origin and differentiation timeline inferred from Ca and Mg stable isotopes. Commun. Earth Environ. 4, 307.

Greber, N.D., Dauphas, N., Puchtel, I.S., Hofmann, B.A., Arndt, N.T., 2017. Titanium stable isotopic variations in chondrites, achondrites and lunar rocks. Geochim. Cosmochim. Acta 213, 534–552.

Hammer, J.E., 2006. Influence of f_{O_2} and cooling rate on the kinetics and energetics of Fe-rich basalt crystallization. Earth Planet. Sci. Lett. 248, 618–637.

Hess, P.C., Parmentier, E., 1995. A model for the thermal and chemical evolution of the Moon's interior: implications for the onset of mare volcanism. Earth Planet. Sci. Lett. 134, 501–514.

Hoare, L., Klaver, M., Muir, D.D., Klemme, S., Barling, J., Parkinson, I.J., Lissenberg, C.J., Millet, M.A., 2022. Empirical and experimental constraints on Fe-Ti oxide-melt titanium isotope fractionation factors. Geochim. Cosmochim. Acta 326, 253–272.

Jiang, Y., Kang, J., Liao, S., Elardo, S.M., Zong, K., Wang, S., Nie, C., Li, P., Yin, Z., Huang, F., et al., 2023. Fe and Mg isotope compositions indicate a hybrid mantle source for young Chang'E 5 mare basalts. Astrophys. J. Lett. 945, L26.

Johannes, W., Bell, P., Mao, H., Boettcher, A., Chipman, D., Hays, J., Newton, R., Seifert, F., 1971. An interlaboratory comparison of piston-cylinder pressure calibration using the albite-breakdown reaction. Contrib. Mineral. Petrol. 32, 24–38.

Johnson, A.C., Aarons, S.M., Dauphas, N., Nie, N.X., Zeng, H., Helz, R.T., Romaniello, S.J., Anbar, A.D., 2019. Titanium isotopic fractionation in Kilauea Iki lava lake driven by oxide crystallization. Geochim. Cosmochim. Acta 264, 180–190.

Klaver, M., Luu, T.H., Lewis, J., Jansen, M.N., Anand, M., Schwieters, J., Elliott, T., 2021. The Ca isotope composition of mare basalts as a probe into the heterogeneous lunar mantle. Earth Planet. Sci. Lett. 570, 117079.

Kommescher, S., Fonseca, R., Kurzweil, F., Thiemens, M., Münker, C., Sprung, P., 2020. Unravelling lunar mantle source processes via the Ti isotope composition of lunar basalts. Geochem. Perspect. Lett. 13, 13–18.

Krawczynski, M.J., Grove, T.L., 2012. Experimental investigation of the influence of oxygen fugacity on the source depths for high titanium lunar ultramafic magmas. Geochim. Cosmochim. Acta 79, 1–19.

Leitzke, F., Fonseca, R., Göttlicher, J., Steininger, R., Jahn, S., Prescher, C., Lagos, M., 2018. Ti K-edge XANES study on the coordination number and oxidation state of titanium in pyroxene, olivine, armalcolite, ilmenite, and silicate glass during mare basalt petrogenesis. Contrib. Mineral. Petrol. 173, 1–17.

Li, H., Zhang, N., Liang, Y., Wu, B., Dygert, N.J., Huang, J., Parmentier, E., 2019. Lunar cumulate mantle overturn: a model constrained by ilmenite rheology. J. Geophys. Res., Planets 124, 1357–1378.

Lin, Y., Hui, H., Xia, X., Shang, S., van Westrenen, W., 2020. Experimental constraints on the solidification of a hydrous lunar magma ocean. Meteorit. Planet. Sci. 55, 207–230.

Lin, Y., Tronche, E.J., Steenstra, E.S., van Westrenen, W., 2017a. Evidence for an early wet Moon from experimental crystallization of the lunar magma ocean. Nat. Geosci. 10, 14–18.

Lin, Y., Tronche, E.J., Steenstra, E.S., van Westrenen, W., 2017b. Experimental constraints on the solidification of a nominally dry lunar magma ocean. Earth Planet. Sci. Lett. 471, 104–116.

Liu, J., Dauphas, N., Roskosz, M., Hu, M.Y., Yang, H., Bi, W., Zhao, J., Alp, E.E., Hu, J.Y., Lin, J.F., 2017. Iron isotopic fractionation between silicate mantle and metallic core at high pressure. Nat. Commun. 8, 14377.

Liu, Y., Spicuzza, M.J., Craddock, P.R., Day, J.M., Valley, J.W., Dauphas, N., Taylor, L.A., 2010. Oxygen and iron isotope constraints on near-surface fractionation effects and the composition of lunar mare basalt source regions. Geochim. Cosmochim. Acta 74, 6249–6262.

Mallik, A., Ejaz, T., Shcheka, S., Garapic, G., 2019. A petrologic study on the effect of mantle overturn: implications for evolution of the lunar interior. Geochim. Cosmochim. Acta 250, 238–250.

Médard, E., McCammon, C.A., Barr, J.A., Grove, T.L., 2008. Oxygen fugacity, temperature reproducibility, and H_2O contents of nominally anhydrous piston-cylinder experiments using graphite capsules. Am. Mineral. 93, 1838–1844.

Millet, M.A., Dauphas, N., 2014. Ultra-precise titanium stable isotope measurements by double-spike high resolution MC-ICP-MS. J. Anal. At. Spectrom. 29, 1444–1458.

Millet, M.A., Dauphas, N., Greber, N.D., Burton, K., Dale, C., Debret, B., Macpherson, C., Nowell, G., Williams, H.M., 2016. Titanium stable isotope investigation of magmatic processes on the Earth and Moon. Earth Planet. Sci. Lett. 449, 197–205.

Neal, C.R., Taylor, L.A., Lindstrom, M.M., 1988. Apollo 14 mare basalt petrogenesis-assimilation of KREEP-like components by a fractionating magma. In: Lunar and Planetary Science Conference Proceedings, pp. 139–153.

Ni, P., Zhang, Y., Fiege, A., Newville, M., Lanzirotti, A., 2021. Rapid reduction of basaltic glasses in piston-cylinder experiments: a XANES study. Contrib. Mineral. Petrol. 176, 1–18.

Nie, N.X., Dauphas, N., Alp, E.E., Zeng, H., Sio, C.K., Hu, J.Y., Chen, X., Aarons, S.M., Zhang, Z., Tian, H.C., et al., 2021. Iron, magnesium, and titanium isotopic fractionations between garnet, ilmenite, fayalite, biotite, and tourmaline: results from NRIXS, ab initio, and study of mineral separates from the Moosilauke metapelite. Geochim. Cosmochim. Acta 302, 18–45.

Poitrasson, F., Zambardi, T., Magna, T., Neal, C.R., 2019. A reassessment of the iron isotope composition of the Moon and its implications for the accretion and differentiation of terrestrial planets. Geochim. Cosmochim. Acta 267, 257–274.

Polyakov, V., Mineev, S., Clayton, R., Hu, G., Mineev, K., 2005. Determination of tin equilibrium isotope fractionation factors from synchrotron radiation experiments. Geochim. Cosmochim. Acta 69, 5531–5536.

Prissel, K., Olive, J.A., Krawczynski, M.J., 2023. A log-ratio-based algorithm for petrologic mass-balance problems and uncertainty assessment. Geochem. Geophys. Geosyst. 24, e2023GC011234.

Prissel, K.B., 2020. Experimental Constraints on Igneous Iron Isotopic Fractionation and Diffusion. Ph.D. thesis. Washington University in St. Louis.

Prissel, K.B., Krawczynski, M.J., Nie, N.X., Dauphas, N., Couvy, H., Hu, M.Y., Alp, E.E., Roskosz, M., 2018. Experimentally determined effects of olivine crystallization and melt titanium content on iron isotopic fractionation in planetary basalts. Geochim. Cosmochim. Acta 238, 580–598.

Prissel, K.B., Krawczynski, M.J., Van Orman, J.A., 2020. Fe–Mg and Fe–Mn interdiffusion in ilmenite with implications for geospeedometry using oxides. Contrib. Mineral. Petrol. 175, 1–17.

Rapp, J., Draper, D., 2018. Fractional crystallization of the lunar magma ocean: updating the dominant paradigm. Meteorit. Planet. Sci. 53, 1432–1455.

Rzehak, L.J., Kommescher, S., Hoare, L., Kurzweil, F., Sprung, P., Leitzke, F.P., Fonseca, R.O., 2022. Redox-dependent Ti stable isotope fractionation on the Moon: implications for current lunar magma ocean models. Contrib. Mineral. Petrol. 177, 81.

Rzehak, L.J., Kommescher, S., Kurzweil, F., Sprung, P., Leitzke, F.P., Fonseca, R.O., 2021. The redox dependence of titanium isotope fractionation in synthetic Ti-rich lunar melts. Contrib. Mineral. Petrol. 176, 1–16.

Schauble, E.A., 2011. First-principles estimates of equilibrium magnesium isotope fractionation in silicate, oxide, carbonate and hexaaquamagnesium (2+) crystals. Geochim. Cosmochim. Acta 75, 844–869.

Schmidt, M.W., Kraettli, G., 2022. Experimental crystallization of the lunar magma ocean, initial selenotherm and density stratification, and implications for crust formation, overturn and the bulk silicate Moon composition. J. Geophys. Res., Planets 127, e2022JE007187.

Sedaghatpour, F., Jacobsen, S.B., 2019. Magnesium stable isotopes support the lunar magma ocean cumulate remelting model for mare basalts. Proc. Natl. Acad. Sci. 116, 73–78.

Sedaghatpour, F., Teng, F.Z., Liu, Y., Sears, D., Taylor, L.A., 2013. Magnesium isotopic composition of the Moon. Geochim. Cosmochim. Acta 120, 1–16.

Shearer, C.K., Hess, P.C., Wieczorek, M.A., Pritchard, M.E., Parmentier, E.M., Borg, L.E., Longhi, J., Elkins-Tanton, L.T., Neal, C.R., Antonenko, I., et al., 2006. Thermal and magmatic evolution of the Moon. Rev. Mineral. Geochem. 60, 365–518.

Shervais, J.W., Taylor, L.A., Lindstrom, M.M., 1985. Apollo 14 mare basalts: petrology and geochemistry of clasts from consortium breccia 14321. J. Geophys. Res., Solid Earth 90, C375–C395.

Sio, C.K., Roskosz, M., Dauphas, N., Bennett, N.R., Mock, T., Shahar, A., 2018. The isotope effect for Mg-Fe interdiffusion in olivine and its dependence on crystal orientation, composition and temperature. Geochim. Cosmochim. Acta 239, 463–480.

Sio, C.K.I., Dauphas, N., 2017. Thermal and crystallization histories of magmatic bodies by Monte Carlo inversion of Mg-Fe isotopic profiles in olivine. Geology 45, 67–70.

Sio, C.K.I., Dauphas, N., Teng, F.Z., Chaussidon, M., Helz, R.T., Roskosz, M., 2013. Discerning crystal growth from diffusion profiles in zoned olivine by in situ Mg-Fe isotopic analyses. Geochim. Cosmochim. Acta 123, 302–321.

Snyder, G.A., Taylor, L.A., Neal, C.R., 1992. A chemical model for generating the sources of mare basalts: combined equilibrium and fractional crystallization of the lunar magmasphere. Geochim. Cosmochim. Acta 56, 3809–3823.

Sossi, P.A., Moynier, F., 2017. Chemical and isotopic kinship of iron in the Earth and Moon deduced from the lunar Mg-suite. Earth Planet. Sci. Lett. 471, 125–135.

Sossi, P.A., O'Neill, H.S.C., 2017. The effect of bonding environment on iron isotope fractionation between minerals at high temperature. Geochim. Cosmochim. Acta 196, 121–143.

Stadermann, A.C., Jolliff, B.L., Krawczynski, M.J., Hamilton, C.W., Barnes, J.J., 2022. Analysis and experimental investigation of Apollo sample 12032, 366-18, a chemically evolved basalt from the Moon. Meteorit. Planet. Sci.

Sturhahn, W., Alp, E., Quast, K., Toellner, T., 1999. Lamb-Mössbauer factor and second-order Doppler shift of hematite. Advanced Photon Source User Activity Report.

Teng, F.Z., Dauphas, N., Helz, R.T., 2008. Iron isotope fractionation during magmatic differentiation in Kilauea Iki lava lake. Science 320, 1620–1622.

Teng, F.Z., Dauphas, N., Helz, R.T., Gao, S., Huang, S., 2011. Diffusion-driven magnesium and iron isotope fractionation in Hawaiian olivine. Earth Planet. Sci. Lett. 308, 317–324.

Thacker, C., Liang, Y., Peng, Q., Hess, P., 2009. The stability and major element partitioning of ilmenite and armalcolite during lunar cumulate mantle overturn. Geochim. Cosmochim. Acta 73, 820–836.

Tian, H.C., Zhang, C., Teng, F.Z., Long, Y.J., Li, S.G., He, Y., Ke, S., Chen, X.Y., Yang, W., 2019. Diffusion-driven extreme Mg and Fe isotope fractionation in Panzhihua ilmenite: implications for the origin of mafic intrusion. Geochim. Cosmochim. Acta.

Van Orman, J.A., Grove, T.L., 2000. Origin of lunar high-titanium ultramafic glasses: constraints from phase relations and dissolution kinetics of clinopyroxene-ilmenite cumulates. Meteorit. Planet. Sci. 35, 783–794.

Van Orman, J.A., Krawczynski, M.J., 2015. Theoretical constraints on the isotope effect for diffusion in minerals. Geochim. Cosmochim. Acta 164, 365–381.

Vander Kaaden, K.E., Agee, C.B., McCubbin, F.M., 2015. Density and compressibility of the molten lunar picritic glasses: implications for the roles of Ti and Fe in the structures of silicate melts. Geochim. Cosmochim. Acta 149, 1–20.

Wagner, T., Grove, T., 1997. Experimental constraints on the origin of lunar high-Ti ultramafic glasses. Geochim. Cosmochim. Acta 61, 1315–1327.

Walker, D., Longhi, J., Stolper, E.M., Grove, T.L., Hays, J.F., 1975. Origin of titaniferous lunar basalts. Geochim. Cosmochim. Acta 39, 1219–1235.

Wang, K., Jacobsen, S.B., Sedaghatpour, F., Chen, H., Korotev, R.L., 2015. The earliest Lunar Magma Ocean differentiation recorded in Fe isotopes. Earth Planet. Sci. Lett. 430, 202–208.

Wang, W., Huang, S., Huang, F., Zhao, X., Wu, Z., 2020. Equilibrium inter-mineral titanium isotope fractionation: implication for high-temperature titanium isotope geochemistry. Geochim. Cosmochim. Acta 269, 540–553.

Wang, W., Wu, Z., Huang, S., Huang, F., 2023. First-principles investigation of equilibrium magnesium isotope fractionation among mantle minerals: review and new data. Earth-Sci. Rev. 104315.

Warren, P.H., 1985. The magma ocean concept and lunar evolution. Annu. Rev. Earth Planet. Sci. 13, 201–240.

Watson, E., Wark, D., Price, J., Van Orman, J., 2002. Mapping the thermal structure of solid-media pressure assemblies. Contrib. Mineral. Petrol. 142, 640–652.

Watson, E.B., Liang, Y., 1995. A simple model for sector zoning in slowly grown crystals: implications for growth rate and lattice diffusion, with emphasis on accessory minerals in crustal rocks. Am. Mineral. 80, 1179–1187.

Weyer, S., Anbar, A.D., Brey, G.P., Münker, C., Mezger, K., Woodland, A.B., 2005. Iron isotope fractionation during planetary differentiation. Earth Planet. Sci. Lett. 240, 251–264.

Zhao, Y., De Vries, J., van den Berg, A., Jacobs, M., van Westrenen, W., 2019. The participation of ilmenite-bearing cumulates in lunar mantle overturn. Earth Planet. Sci. Lett. 511, 1–11.